TECHNISCHE UNIVERSITÄT WIEN

Master Thesis

Experimental study on the feasibility of falling film absorbers for dehumidification in cold stores

zur Erlangung des akademischen Grades

Diplom-Ingenieur

im Rahmen des Studiums

Technische Physik

eingereicht von

Ben Leon Lancelot Stephani

Matrikelnummer 1527025

ausgeführt am
Institut für angewandte Physik(IAP)
an der
Technischen Universität (TU) Wien
in Kooperation mit dem Austrian Institute of Technology (AIT)

Betreuung: Ao. Univ.Prof. Dipl.-Ing. Dr.techn. Martin Gröschl
Privatdoz. Dipl.-Ing. Dr.techn. Christoph Reichl

.....	.....	.....
(Ort, Datum)	(Unterschrift Verfasser)	(Unterschrift Betreuer)

TECHNISCHE UNIVERSITÄT WIEN

Ich habe zur Kenntnis genommen, dass ich zur Drucklegung meiner Arbeit unter der Bezeichnung

Diplomarbeit

nur mit Bewilligung der Prüfungskommission berechtigt bin.

Ich erkläre weiters an Eides statt, dass ich meine Diplomarbeit nach den anerkannten Grundsätzen für wissenschaftliche Abhandlungen selbständig ausgeführt habe und alle verwendeten Hilfsmittel, insbesondere die zugrunde gelegte Literatur genannt habe.

Weiters erkläre ich, dass ich dieses Diplomarbeitsthema bisher weder im In- noch Ausland (einer Beurteilerin/einem Beurteiler zur Begutachtung) in irgendeiner Form als Prüfungsarbeit vorgelegt habe und dass diese Arbeit mit der vom Begutachter beurteilten Arbeit übereinstimmt.

Wien, am 18.10.2024 _____

Kurzfassung

Frostbildung an Luftkühlern in Kühlhäusern verringert die Energieeffizienz des Kühlprozesses erheblich. Sie blockiert den Luftstrom, isoliert die Oberfläche des Luftkühlers und die erforderlichen Abtauzyklen übertragen letztlich unvermeidbar Wärme an den Kühlraum. Die Literatur zeigt, dass durch ein Verhindern der Frostbildung durch Frostschutzmaßnahmen mehr als 15 % der für die Kühlung erforderlichen Energie eingespart werden kann. In dieser Arbeit wird eine experimentelle Untersuchung eines neuartigen Ansatzes zur Verhinderung der Frostbildung an den Luftkühlern in Kühlhäusern vorgestellt. Die vorgeschlagene Lösung verwendet einen Fallfilmabsorber mit flüssigem Absorptionsmittel zur Entfeuchtung der Luft. Dadurch wird die Taupunkttemperatur der Luft vor dem Luftkühler unter die Oberflächentemperatur des Kühlers gesenkt. Somit kondensiert kein Wasser an dessen Oberfläche und es bildet sich kein Frost. Derzeitig übliche Absorptionsmittel wie LiCl und LiBr haben das Problem, dass sie bei niedrigen Temperaturen und hohen Konzentrationen kristallisieren. Außerdem kann es bei der Verwendung mit Metallen zu Korrosion kommen. Um diese Probleme zu vermeiden, wird eine ionische Flüssigkeit verwendet. Durch Verwendung der Abwärme des Kühlsystems ist keine zusätzliche Wärmequelle für die Regeneration des Absorptionsmittels erforderlich. Um die Machbarkeit dieses Ansatzes zu demonstrieren, wurden zwei Lamellenwärmeübertrager durch eigens gefertigte 3D-Druckteile in Fallfilmabsorber umgewandelt. Um die Vorteile und Grenzen des Absorbers und Regenerators zu testen und die Wirksamkeit der Absorption und Regeneration des flüssigen Absorptionsmittels zu bewerten, wurde ein Prüfstand konstruiert, der in der Lage ist die Luft am Eintritt des Absorbers zu konditionieren. Die Ergebnisse zeigen die Funktionsfähigkeit des Fallfilmabsorbers, mit dem der Taupunkt der einströmenden Luft bei 7 °C und 80 % relativer Luftfeuchtigkeit auf -2,5 °C gesenkt werden konnte. Die Experimente zeigten, dass das Absorptionsmittel auch bei 0 °C noch einen fallenden Film bilden kann und dass die Verschleppung von Absorptionsmittel in die Luft bei Geschwindigkeiten unter 2 m/s kein Problem darstellt. Die Regeneration des Absorptionsmittels konnte be Lufttemperaturen von 30 °C und Luftfeuchtigkeit von 40 % erreicht werden, wobei das Absorbtionsmittel auf 42 °C erhitzt wurde. Die Ergebnisse dieser experimentellen Untersuchung zeigen, dass Fallfilmabsorber in der Lage sind die Luft in Kühlhäusern zu entfeuchten und dadurch die Frostbildung an den Luftkühlern und eine damit notwendige Abtauung zu verhindern.

Abstract

Frost formation on air coolers in cold stores significantly reduces the energy efficiency of the refrigeration process. It blocks the airflow, insulates the air cooler surface, and ultimately transfers heat to the cold store due to the required defrosting cycles. According to literature, frost prevention can save more than 15 % of the required energy for refrigeration. This work presents an experimental investigation of a novel approach to prevent frost formation on the air coolers in cold stores. The proposed solution uses a liquid desiccant falling film absorber to dehumidify the air. By this, the dew point temperature of the air upstream of the air cooler is lowered below the surface temperature of the cooler. As a result, no water is condensing on its surface and thereby no frost is formed. Current liquid desiccants, such as LiCl and LiBr, have the problem of crystallization at low temperatures and high concentrations. They also cause corrosion when used with metals. To avoid these problems, an ionic liquid is used as the desiccant. By using the waste heat from the refrigeration system to regenerate the desiccant, no additional heat source is required. To demonstrate the feasibility of this approach, two finned heat exchangers were transformed into falling film absorbers using selfmade 3D printed parts. A test rig was constructed, capable of conditioning the air, testing the advantages and limitations of this method and evaluating the effectiveness of the liquid desiccant absorption and regeneration. The results show the viability of the falling film absorber, where it was possible to reduce the dew point of incoming air at 7 °C and 80 % relative humidity to -2.5 °C. The system showed that the desiccant can still form a falling film at around 0°C and that carry over of desiccant into the air is not an issue at air speeds up to 2 m/s. The regeneration could be achieved at air temperatures of 30 °C with relative humidity of 40 % while the desiccant was heated to 42 °C. The results of this experimental investigation show that it is possible for the liquid desiccant falling film absorber to prevent frost formation on the air coolers, reducing the need for defrosting.

Nomenclature

Abbreviations

AC	Alternating current
AIT	Austrian institute of technology
CAD	Computer-aided design
CFD	Computational fluid dynamics
DC	Direct current
DKV	Deutsche Kälte- und Klimatagung
HEPA	High efficiency particulate air
PLA	Polylactic acid

B	Magnetic field	T
F	Force	kgm/s^2
q	Charge	As

Greek Symbols

χ	Mass ratio	1
η	Dynamic viscosity	$kg/(ms)$
ω	Circular frequency	$1/s$
ρ	Density	kg/m^3

Latin Symbols

$\dot{m}$	Mass flow rate	kg/s
$\dot{Q}$	Heat flow rate	W
c	Specific heat capacity	J/(kgK)
D	Diameter	m
d	Characteristic dimension	m
f	Frequency	1/s
f_D	Darcy friction factor	1
I	Electrical current	A
k	Spring constant	N/m
L	Length	m
m	Mass	kg
p	Pressure	Pa or bar
Q	Heat	J or Wh
R	Resistance	Ω
Re	Reynolds number	1
RH	Relative humidity	1
Sr	Strouhal number	1
T	Temperature	K
U	Voltage	V
V	Volume	m^3
v	Velocity	m/s

Subscripts

a	Air
d	Desiccant
H	Hole
h	Height
L	Level
l	Liquid
s	Solution
tot	Total
w	Wire

Contents

1 Introduction

The condensation of water onto the fins of air coolers in cold stores is a common problem, as it leads to the buildup of frost. As the frost builds up over time, it reduces the efficiency of the heat exchanger by acting as a thermal insulator. In extreme cases it can even cause the pressure drop of the air to increase to a point, where it significantly reduces the air flow. A common approach to solve this issue is the introduction of defrosting cycles, where the air cooler is isolated from the cold store and heated until no frost remains. Electrical heating rods or hot refrigerant gas are often used to speed up this process. Regardless how the defrosting is conducted, the heat transferred to the air cooler has to be removed again, to resume operation. These defrosting are responsible for up to 15 % of the cold stores entire energy consumption (14). One improvement to the current method is to dry the air before reaching the air cooler. If the dew point of the air falls below the surface temperature of the coolant entering the heat exchanger, the water wouldn't condensate, removing the need for defrosting. A widely used method of dehumidifying air is through condensation, which would lead to the same problem of frost formation. The use of sorptive methods can prevent this. One possible solution would be adsorption using a desiccant wheel, where the cold air is forced over a granular desiccant placed inside a rotating cylinder. First the desiccant adsorbes water from the air, then spins into a position where the wet desiccant comes into contact with hot air releasing its adsorbed moisture. While using solid state desiccant in a wheel seems promising, it also comes with some limitations. The hot air has to be introduced directly into the desiccant wheel and therefore into the cold store, where it is brought into relatively close contact with the cool air inside. All of the cooling done to the desiccant is lost. Also the regenerating temperatures of the solid desiccant are often too high to reliably be reached using the access heat of typical heat pumps in this sector. Liquid desiccants may overcome a lot of these disadvantages of their solid state counterparts. They are easily transportable, so the desiccant can be regenerated outside the cold store. They can form falling films, where the surface in contact with the air is constantly being replenished, which enables stationary operation. And most importantly, they can be designed to be able to regenerate at relatively low temperatures. Common liquid desiccants include liquid salts like calcium chloride. A problem of liquid salt desiccants is that they are corrosive and can crystallize at low temperatures. A promising candidate for liquid desiccants are ionic liquids, as they are non corrosive and have shown to remain in liquid form at the operating temperatures of most air coolers in cold stores. There are still open questions about the problem of carry over of desiccant into the air, the consistent formation of the falling films, especially at these low temperatures. To answer these questions in this work, two heat exchangers where transformed into a falling film absorber and a regenerator. A test rig was constructed, capable of conditioning the air to common cold store condition. This work contains first measurement results, insights gained in the work with ionic liquids as a liquid desiccant, and a detailed description of the test rig. The results were presented at the DKV meeting 2023 (8).

2 Theory of dehumidification techniques

Controlling the relative humidity in cold stores is essential to maximize the storage life of food. If the relative humidity is too high, an increased growth of microorganisms leads to excessive food spoilage. A low humidity level can result in shriveling and damage to animal tissue (9). Optimal humidity levels vary but are often assumed to be around 80 % (10). These high levels of relative humidity required to maximize the shelf life results in frost formation on the air coolers. It would theoretically be possible, to construct the air coolers in a way, where the contact area is so large, that the temperature of the fins can stay above the dew point temperature, while still providing the required cooling power. This is almost never realized however, due to the high installation cost and the fact that some moisture is constantly being introduced, which has to be removed. What is done instead, is to let the water condensate onto the fins of the air coolers, where it freezes. The frost layer reduces the effectiveness of the air cooler, because of the low thermal conductivity of the ice. The build up of ice also increases the pressure drop over the air cooler, as the rougher surface and thinner gaps can change the flow profile (15). In extreme cases it could even block the flow entirely. To get rid of the ice, defrosting cycles are introduced, where the air exchange between the coolers and the cold store is shut and the cooler is heated until the ice has melted away. The extra energy cost needed to cool the heat exchanger down again combined with the cooling power lost in freezing the ice contributes to about 15 % of the cold stores total power consumption (14). To prevent frost formation on the fins without increasing the size of the air coolers, a solution is dehumidification of the air. There are multiple possibilities to dehumidify air, but the most common mechanisms are condensation and sorption. The air would be dehumidified in front of the air cooler, to the point where the dew point temperature falls below the inlet temperature of the coolant entering the air cooler. That way no water will condensate on the fins, preventing frost formation. There are also some promising results in the research of electrically driven dehumidification technologies, however their current limitations still make them unfeasible for large scale projects (12).

2.1 Condensation

A widely adopted method of dehumidifying air is through condensation. This works by cooling a surface in contact with the air so that the air temperature would fall below its dew point temperature. When the dew point temperature is reached, water starts condensing on the surface giving off latent heat. As further cooling is provided the dew point temperature starts falling together with the air temperature, as further water condensates. The simplicity of this system makes it the method of choice for many applications. This method however is insufficient for the use in cold stores, because normally the dew point temperature is below the freezing point of water. Therefore the condensing water would built a frost layer and the aimed problem would not be solved

but only shifted away from the air cooler.

2.2 Sorption

Sorption of water out of the air can be accomplished either through adsorption or absorption. In the process of adsorption the water creates a film on the surface of another medium, typically a solid, while absorption describes the process of the water entering into a bulk of either a solid or a liquid. The material into or onto which the water is absorbed is called the desiccant. Desiccants can only hold a limited amount of water, before they have to be regenerated. In the case of cold stores, the regeneration process can be accomplished using the waste heat of the heat pumps. Adsorption onto Solid desiccants is typically achieved by the use of a desiccant wheel, while liquid desiccants are either used to create falling films, or sprayed (11).

2.2.1 Adsorption

When solid desiccants are used in cold stores, they are typically mounted inside a wheel, where one section can be connected to the upstream side of the air coolers, to dehumidify the air inside to cold store, and another section to a heat source, where the desiccant is being regenerated. There are multiple different possible options for mounting the desiccant, however the rotating wheel is often to be preferred due to its high compactness, option for continuous cycle and high dehumidification capacity (1). It was shown in simulations, that the performance in greenhouses can be improved with the addition of a desiccant wheel (5). The advantages of solid desiccants lie in the material properties, where they have a high water carrying capacity and are typically non corrosive. The main problem of the desiccant wheel solution is the high thermal conductivity of the system. The hot air has to come physically close to the cooling cycle, and the sections of the wheel have to be insulated properly. Even though these losses can be minimized with proper insulation, the heat losses into the desiccant, which has to continuously be heated and cooled, can not.

To maximize the efficiency of the system, a liquid desiccant cycle can be introduced, where the absorption and regeneration can be separated, and the heat losses to the desiccant can be reduced using a heat exchanger (12).

2.2.2 Absorption

An effective way to create a liquid desiccant-air boundary is through the use of falling film absorbers. The three most common geometries used are in a horizontal tube, a vertical tube and vertical plate arrangement (3). The focus of this work lies in the vertical plate variant. Their construction is similar to that of a common fin and tube heat exchanger, where a thin film of liquid flows down on both sides of the fins. This geometry ensures a large surface area with a high cross flow section of the air, leading to a low air side pressure drop. Liquid salts like LiBr and CaCl are commonly used as desiccant and have shown to perform well in falling film absorbers, especially at low air speeds (6). The common liquid salt desiccants however typically are quite corrosive, which leads to either higher maintenance cost, or higher acquisition costs for higher grade materials and also they have crystallize at low temperatures. Ionic liquids provide a promising alternative, as they have an extremely low vapor pressure, high thermal stability and low corrosion, while being highly soluble (16). There are multiple ways to optimize the properties of the desiccant including different chemical compositions and even introduction of ultra fine Cu particles, to improve thermal conductivity of the film (2). There are numerous CFD-simulations of the behaviors of falling films, however due to the high computational costs required for their simulation, the problem is often significantly simplified. For example the falling films are often considered to be laminar, even though at high Reynolds numbers the films start to form waves, which improve the absorption performance (13). It is therefore of interest, to physically test the performance of falling film absorbers complementary to the simulations.

3 Experimental work

To test the viability of absorption through falling film absorbers in cold stores, two fin and tube heat exchangers from Stemotech were transformed into an absorber and a regenerator. In order to test their performance a test rig was built, where the absorber and the regenerator are each mounted in a closed loop air duct, which is able to condition and transport the air through them. Both air circuits are connected by the desiccant cycle. It consists of two desiccant tanks, one connected to the absorber and one to the regenerator. The tanks can exchange desiccant and a heat exchanger between them helps to minimize thermal losses. The cooling power is provided by a system of two bath thermostats. The main difference between the two falling film absorber is their size with the absorber having about 4 times the entry area of the regenerator.

3.1 Absorber and regenerator

The falling film absorbers were created by modifying fin and tube air heat exchangers. All modifications where 3D printed. The inserts where mounted between each pair of fins at the top as seen in Fig. 1. They where designed to keep a constant distance to each fin in order to create even flow. This was accomplished by adding small nubs on each side, small enough not to interrupt the flow. The circular cutouts snap on the heat exchanger pipes for better stability. The inserts are a bit shorter than the full length of the heat exchanger in order to prevent desiccant carry over into the air. After that two walls were mounted in the front and the back. They connect to the fin inserts by hooking into the small grooves. The inserted walls are sealed tightly with the sides of the heat exchanger using silicon. After that, in order to distribute the desiccant evenly over the fin inserts, a distributor was mounted on top. It consists of multiple holes with nubs at the bottom. At the top there is a hose adapter, connecting it to the desiccant tank. Inside a barrier diverts the incoming beam to redistribute the pressure more evenly.

3.1.1 Geometry of the heat exchanger

The fin and tube heat exchanger consists of multiple fins which are rectangular bisected by the pipes of the tempering liquid. These intersections create massive barriers for the falling film resulting in a varying layer thickness throughout the entire plain. To ensure reformation of the thin film and maximize coverage, the fins are covered with a hydrophilic coating. At the bottom, a drip tray with an outflow is used to prevent desiccant from spilling into the air duct.

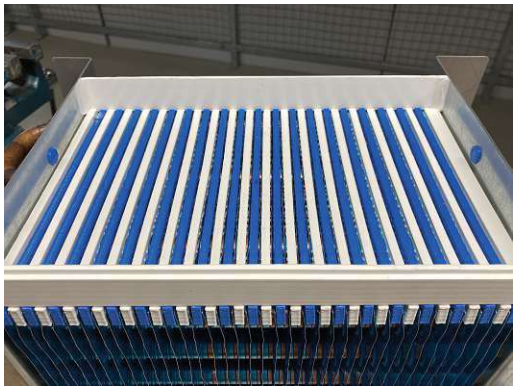

(a) When assembling the absorber, first the inserts and side walls were put in place. The small holes on the sides were plugged using 3D-printed parts. To prevent leakages, everything was sealed using silicone. The two inserts at the ends are thicker than the rest to compensate for the extra space.

(b) The inserts have small hemispheres attached on both sides, keeping the space to the fins even. The flat top was chosen so the desiccant can spread out easily in case of any biases of the distributor. Also, it eased the 3D-printing process.

Figure 1: The inserts inside the absorber help to create laminar flow of the desiccant on the fins.

3.1.2 Inserts

The inserts are covered with small semicircles on both sides as seen in Fig. 1 and Fig. 2. Each of these is 0.7 mm in diameter to ensure constant distance to the fins. The top is flat in order to be 3D printable without supports. They were printed out of polylactic acid (PLA). The circular cutouts at the bottom of the inserts snap on to the copper pipes, adding stability. One of the main concerns was the difference in viscosity of the desiccant at varying temperatures. In order to check the performance of the inserts, the film formation on the regenerator was tested with both water and vegetable oil, simulating the extreme ends of the viscosity spectrum. The inserts performed sufficient in both cases.

3.1.3 Desiccant distributor

The desiccant distributor consists of four parts for the regenerator, shown in Fig. 3 and 9 parts for the absorber, shown in Fig. 4. The reason for this is that even though the principle designs are identical, the size of the print bed required separation of the distributor into multiple parts. All pieces where glued together using superglue. The bottom and side wall connections were reinforced with silicon before gluing the top. The bottom piece was printed upside down. This made it possible to position tare off nubs

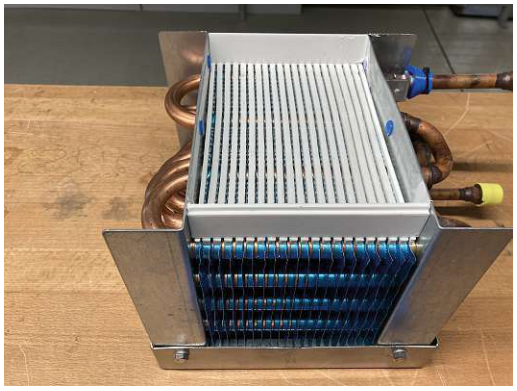

(a) The regenerator was assembled similarly to the absorber. The only difference being the size, position of the heating pipes and number of fins. On the right side the blue cones on the inlet pipes are used create a seal at the air duct.

(b) The inerts for the regenerator are constructed in a similar way to the ones for the absorber. The main difference is the cutout at the back side, as the layout of the copper pipes differs.

Figure 2: Backside of the regenerator with insert.

at every hole, preventing the droplets from shifting on the bottom. The grooves on the bottom connect to the two side plates at the top of each falling film absorber, as well as the 2 PLA side walls. The holes in the bottom form a non rectangular grid so that no single line of holes would be mounted directly on top of a single heat exchanger fin. The side walls have grooves, easing assembly and adding strength. The top part has a nozzle directly in the center, connecting to the inlet hose.

In order to test the distributors, they were connected to a water source (Fig. 5). At low water pressures the distribution is not very homogeneous and responds to small changes in tilt. This effect however diminishes with higher pressures. This can be explained by the decrease of relative pressure contributed by gravity compared to the pressure at the inlet. As the desiccant has a higher viscosity than water, the desiccant pumps have to generate even higher pressure in order to achieve similar flow to the test, increasing the effect. The pressure drop over a the length of a cylindrical hole assuming laminar flow is described by the Darcy–Weisbach equation:

$$\frac{\Delta p_H}{L} = f_D \frac{\rho \langle v \rangle^2}{2D} \tag{1}$$

Here Δp_H is the pressure drop over the length of the hole L and diameter D. The density ρ and the Darcy friction factor f_D which is inversely proportional to the Reynolds number are material properties of the desiccant. As the pressure drop depends on the square of the mean flow velocity $\langle v \rangle$, the flow rate only depends on the root of the total pressure. The addition of the beam stopper drastically reduces dynamic effects on the

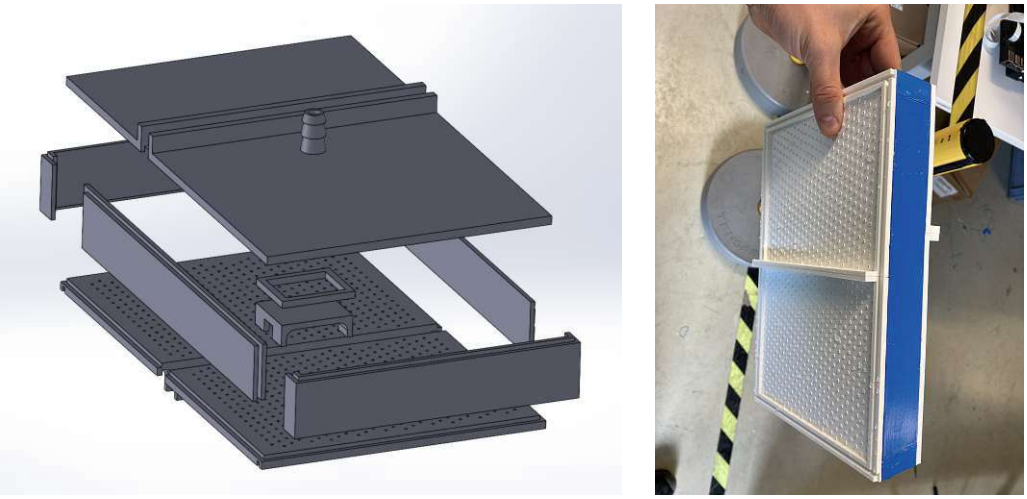

(a) The absorber distributor consists of 8 main parts, which are all glued together. The reason for this is the limiting size of the print bed. The latches between the 2 bottom and top parts ensure a large area for applying the adhesive.

(b) The fully assembled distributor for the absorber has groves on the bottom, to attach to the printed side walls and the metal frame at the top of the absorber.

Figure 3: Absorber distributor design and prototype.

pressure difference at each nub. Considering only gravitational effect of a slightly tilted distributor, the relative difference in pressure at two nobs at different desiccant levels is given by:

$$\frac{\Delta p}{p_{tot}} = \frac{p_{L1} - p_{L2}}{p_{pump} + p_{h1}} \tag{2}$$

Here Δp describes the difference in pressure due to the difference in level height p_{L1} and p_{L2} at two nubs on opposite ends of the distributor. The total pressure p_{tot} at nub 1 depends on the gravitational pressure and the pressure provided by the pump p_{pump} at the inlet of the distributor. At high viscosity and flow rates, this term dominates the gravitational effect. Since the flow rate at each nub depends on the root of the local pressure and the differences in local pressure diminish at operating conditions, the large reactions during the test with water at low pressures does not cause concerns.

Once the performance of the distributors and the inserts were tested successfully, all parts were glued in place and additionally sealed with silicone. The assembly process for the absorber and regenerator is shown in Fig. 6 and Fig. 7.

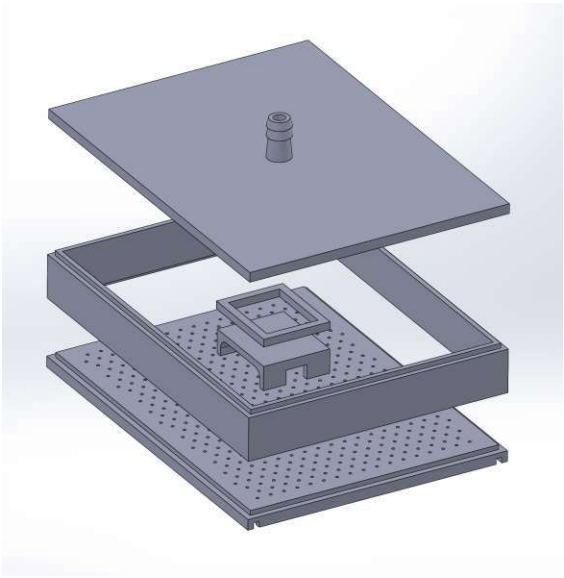

(a) The distributor of the regenerator consist of 3 main parts glued together. The groves at the bottom connect to the walls at the top of the regenerator. Inside, a small beam stopper diverts the incoming desiccant to even out the pressure on the distribution holes at the bottom.The top part connects directly to the desiccant inlet hose.

(b) The absorber distributor fully assembled as seen from the bottom. The small tear off nubs at the bottom prevent traveling of the droplets.

Figure 4: Regenerator distributor design and prototype.

(a) The absorber distributor.

(b) The regenerator distributor.

Figure 5: Performance tests of the distributors using water. Small changes in tilt worsens the performance notably. However, this effect reduces with increasing pressure at the inlet.

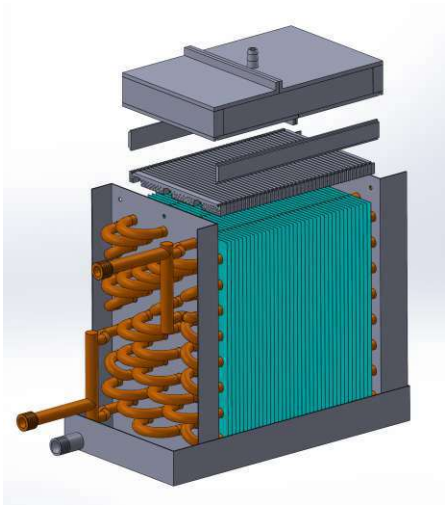

(a) Explosion rendering of the absorber and all 3D-printed parts.

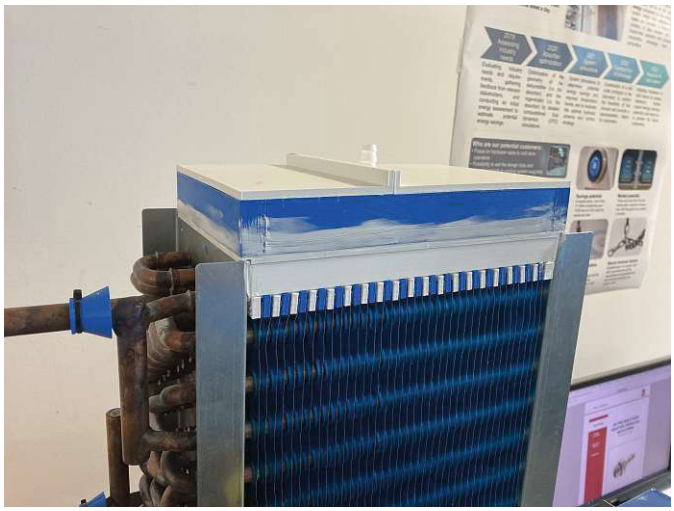

(b) Front of the fully assembled absorber.

Figure 6: While the fin inserts are just snapped onto the copper pipes all other parts of the absorber are glued together and sealed using silicone.

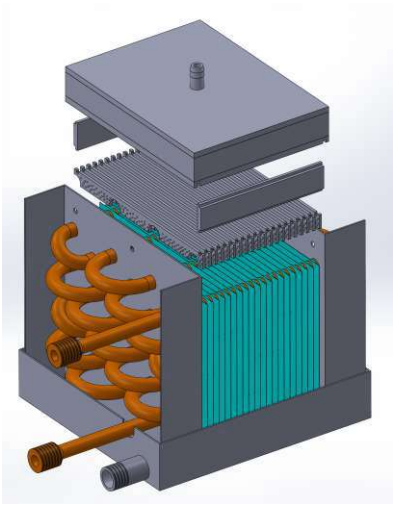

(a) Explosion rendering of the regenerator.

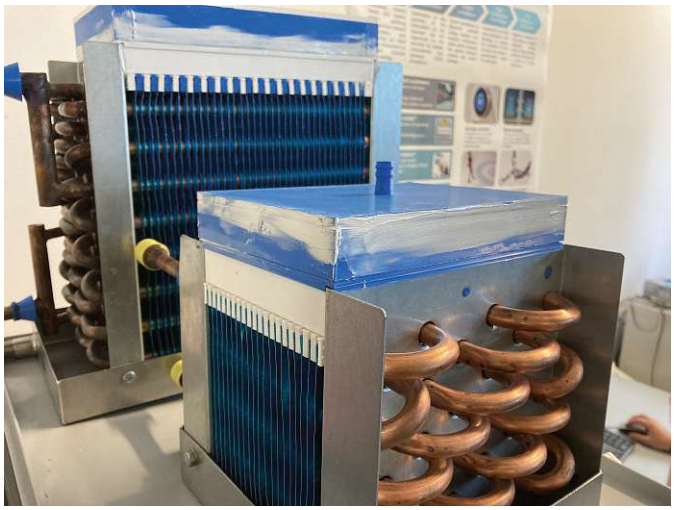

(b) The regenerator in the front with the absorber in the back.

Figure 7: The regenerator was assembled similarly to the absorber.

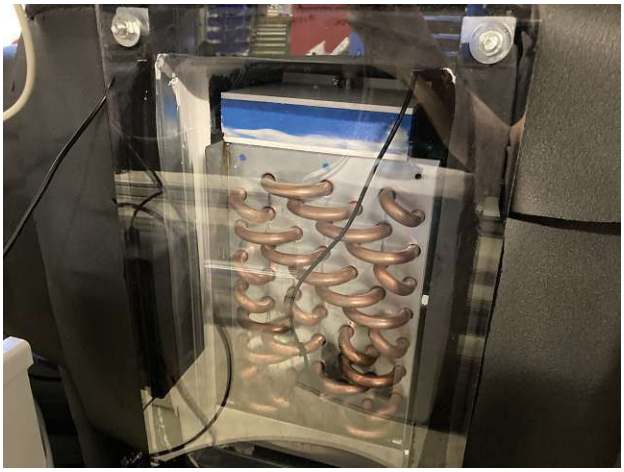

(a) The installed absorber as seen from the outside: The black cable connects to a liquid sensor inside the drip tray, which shuts off the desiccant pump supply when triggered. A 3D-printed plastic piece holds the absorber in place.

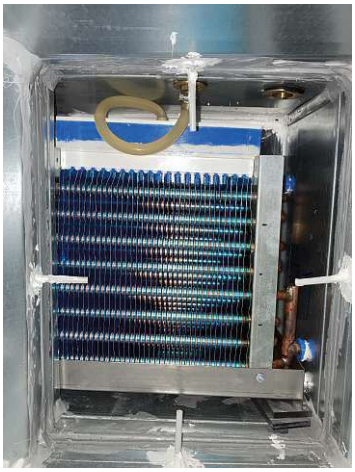

(b) The absorber backside as seen from inside the air duct: The four plastic tubes connect to a differential pressure sensor to measure the pressure drop over the absorber.

Figure 8: The absorber mounted inside the air duct as seen from the side and the back. The frontside of the absorber connects to a window in the plexiglass sheet at the front, forcing all the air through the fins.

3.1.4 Installation

The installed absorber is shown in Fig. 8. To connect the absorber and regenerator to the tempering and desiccant sources, holes were drilled into the back side of the air ducts. An acrylic glass plate was mounted inside the air duct vertically to the flow direction. It has a cut out window of the same size as the entry area of the absorber/regenerator. The absorber and regenerator were then mounted slightly elevated connecting to the acrylic glass window. This has the advantage of a leakage being easily detectable, as the bottom of the duct can be observed from the outside. The three holes on the backside of the duct were used to install the desiccant outlet and cooling/heating connections. They were sealed using 3D printed cones and silicone. The desiccant inlet is positioned at the top and is realized by a tank fitting. A fluid sensor is mounted on the tray at the bottom, acting as an additional safety measure. It immediately stops the desiccant supply pumps when active, preventing of the desiccant into the air duct.

In order to validate the performance of the absorber and regenerator, a test rig was build (Fig. 9). It is divided into two sections. One absorption side, used to test the performance of the absorber and one desorption side, used to test the regenerator. Both sides consist of air ducts including airtight loops made from common air ducts. On both loops there

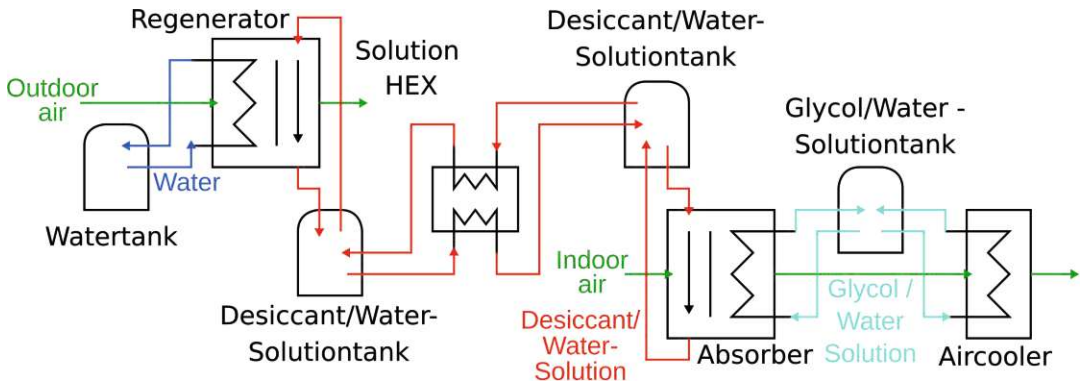

Figure 9: Schematic of how the system could look like in an actual cold store. On the bottom right side the cold air gets dehumidified before reaching the air cooler, preventing condensation and thus frost formation. The water enriched desiccant is then transferred to the absorber tank (top right Desiccant/Water-Solutiontank). This tank exchanges its water rich desiccant with the regenerator tank (bottom left Desiccant/Water-Solutiontank). On the top left side the desiccant gets regenerated using outdoor air. In the test rig however, the air inlets and outlets represented by the green arrows form closed loops.

are multiple components for conditioning the air. The absorber and the regenerator loop are connected by the desiccant system. In order to reduce thermal losses, all air ducts are wrapped in insulation material. Beneath both the absorber and the regenerator there are tanks holding the liquid desiccant. From these desiccant tanks the ionic liquid can be pumped to the absorber/regenerator. The desiccant can also be exchanged between the two tanks. To minimize heat losses, a heat exchanger is positioned between them. The cooling cycle is driven by 2 bath thermostats filled with an ethylene glycol water solution as the coolant. The coolant is distributed to the air cooler on the hot side and the absorber and air cooler on the cold side through a manifold. Each device is connected to a pump group for controlling the temperature. Multiple sensors are mounted in the air duct as well as at the inlets and outlets of the heat exchangers. A CAD drawing and the fully assembled test rig are shown in Fig. 10.

3.2 Dehumidification/absorption

On the absorber section, the absorber is mounted upstream of the air cooler with the goal to dehumidify enough, to prevent frost formation. Fig. 11 shows a schematic of the air duct. Between them two air filters are positioned to check for unwanted ablation of the desiccant. The first filter is a rough G4 filter and the second a highly efficient H14 HEPA-filter. Further upstream of the absorber an air heater is used to control the

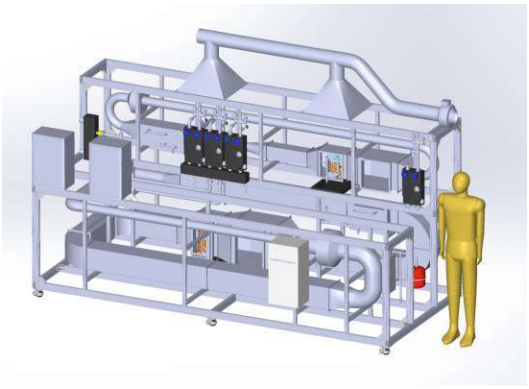

(a) Design of the test rig with dummy for size comparison.

(b) The finished test rig with insulation.

Figure 10: The test rig consists of two separate air ducts: The absorber section on the bottom and the regenerator section on top.

temperature, as well as a steam humidifier and an ultrasonic humidifier to control the humidity of the system. Between the air heater and the humidifiers a flow straightener creates laminar flow. This is needed for an accurate measurement of the anemometer. A single fan is used to drive the system, which is mounted between the humidifiers. Multiple temperature and humidity sensors are mounted throughout the air duct as well as a hot wire anemometer to measure flow velocity, thus being able to calculate the mass flow rate of the air flow. The distances between conditioning and measuring the air were mostly chosen to be sufficiently long to ensure proper mixing. However, to prevent measurement errors due to heat losses to the surroundings, the temperature sensors downstream of the falling film absorbers and heat exchangers are positioned relatively close. To compensate the potential non-uniformity in these cases, three temperature sensors were positioned at different heights in these positions.

3.3 Regeneration/desorption

On the regenerator section, a heating element controls the temperature at the regenerator entrance as seen in Fig. 12. Upstream of it an air cooler is used to control the humidity at the regenerator inlet. A sufficiently large distance between the air heater and the absorber ensures proper mixing of the air. Downstream of the regenerator the air moves through two particle filters just like the ones in the absorber section. These filters can be replaced and checked for desiccant carry over. After the filters, a flow straightener is placed to create laminar flow. This is important for the air mass flow measurement of the hot wire anemometer further downstream. A fan is mounted upstream of the air cooler driving the system.

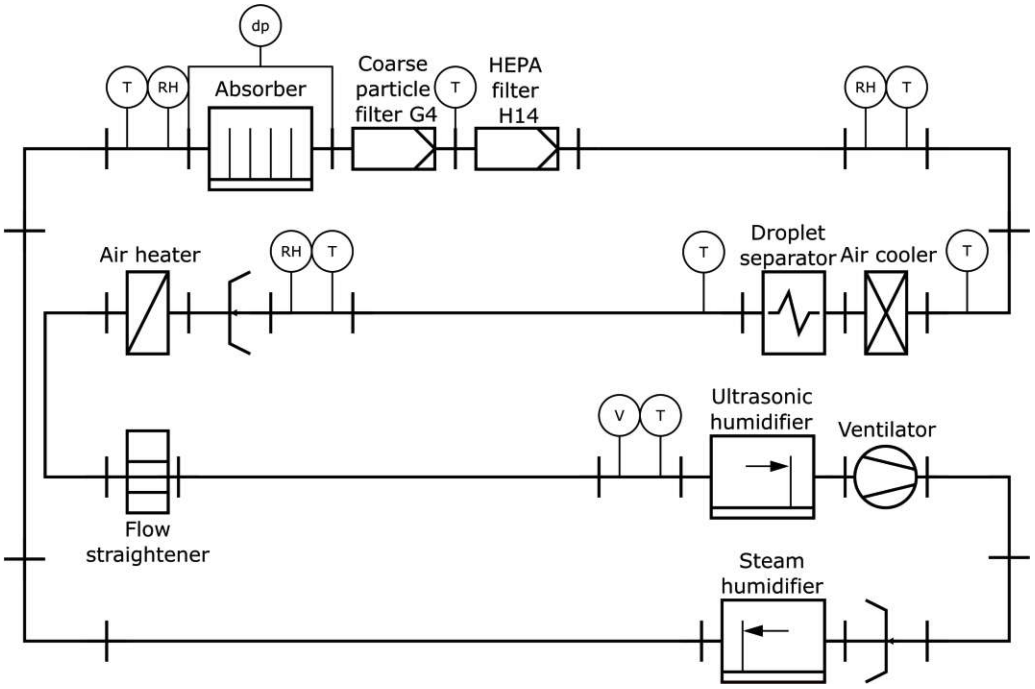

Figure 11: The absorption section: Temperature sensors (T) are mounted upstream and downstream of the absorber and air cooler. Also, next to each relative humidity sensor (RH) another temperature sensor is placed to calculate the absolute water content in the air. A differential pressure sensor (dp) measures the pressure drop over the absorber and a hot wire anemometer (V) is used to measure the flow velocity of the air.

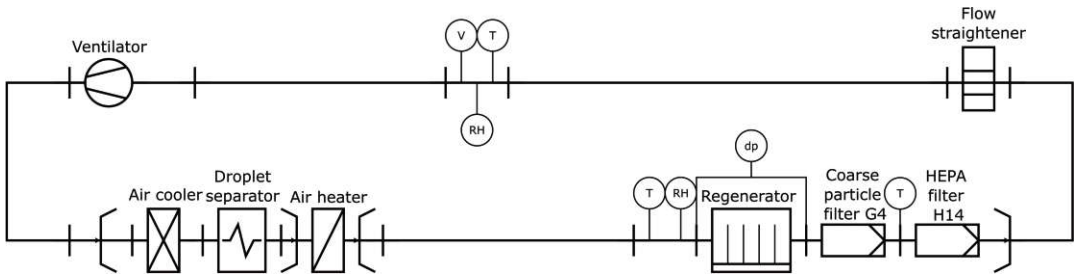

Figure 12: The regeneration section: Temperature sensors (T) are mounted upstream and downstream of the regenerator and next to all the relative humidity sensors (RH). To measure the pressure drop over the regenerator a differential pressure sensor (dp) connects to both sides of the air duct. A hot wire anemometer(V) is used to measure the air velocity.

3.4 Desiccant cycle

The desiccant cycle consists of two tanks, a heat exchanger, and 5 pumps (Fig. 13). Each tank has two outlets, two inlets and one direct connection to the air duct to prevent pressure build up inside the tanks. The tanks were created from two 10 liter wide-mouth canisters. Wide mouth canisters were chosen, for easier assembly. The two outlets are positioned at the front of the tank with tank fittings that have extensions reaching to the bottom of the tank. These canisters are placed in a plastic tray beneath each falling film absorber. At each tank outlet the system is driven by a brush less DC gear pump, which then leads to a Coriolis mass flow sensor. One tank outlet is connected to the heat exchanger and flows into the inlet at the top of the other tank. The other outlet connects through a tank fitting on top of the air duct to the absorber/regenerator. Since the regenerator is mounted higher than the absorber, the back flow can be powered by gravity alone. A simple hose connects the regenerator outlet to the top of the tank. For the absorber only a few centimeters in height difference are not enough to ensure a large enough back flow rate, so a brush less DC paddle wheel pump is connected in between the absorber outlet and the top of the tank. This pump is non regulated and wired in a way that it is always turned on with the desiccant pump power supply. In order to measure the level in each desiccant tank, a level sensor was inserted. The direct connection to the air duct was connected at the top of the tank. Without this connection, the system would have a problem. The gear pumps are self sealing. Once after shutting them down, the desiccant in the collection tray of the absorber and regenerato, would be blocked from rinsing back into the tank. The air in the tank would have nowhere to escape. This would be especially problematic on the absorber side, since the paddle wheel pump would be pressurizing the tank. In addition the tanks could be pressurized when exchanging desiccant between the tanks.

The mass flow of the desiccant between the absorber tank and the regeneration tank, will in general not be equal. One reason for this is the difference in water concentration in the mixture flowing in each direction. In continuous operation the desiccant mass flow would have to be constant, not the one of the mixture. This results in a higher mass flow of the mixture from the absorber tank to the regenerator tank. However, the capability of increasing or decreasing the amount of desiccant in a single tank, without opening the system, was also important for operating the test rig. The only way the access air can escape a tank is into the air duct. The additional air put into the air duct does not cause any concerns, as the ducts are not perfectly sealed. When the system is in continuous operation the mass flow of the desiccant water solution in each direction differs:

$$\dot{m}_{d(in)} = \dot{m}_{d(out)} \tag{3}$$

$$\dot{m}_{s(in)}\chi_{d(in)} = \dot{m}_{s(out)}\chi_{d(out)} \tag{4}$$

The mass flow of the desiccant into ($\dot{m}_{d(in)}$) and out ($\dot{m}_{d(out)}$) of each tank must be the same for continuous operation. As the concentrations of the desiccant in the two tanks

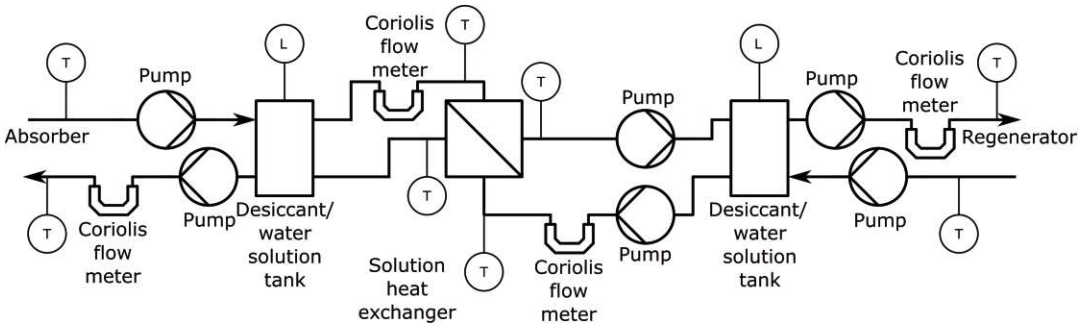

Figure 13: The desiccant cycle consists of two tanks, each with a level sensor (L). Between the tanks the desiccant is exchanged through a solution heat exchanger. Temperature sensors (T) are positioned a both inlet and outlet of the heat exchanger and the absorber and regenerator Coriolis flow sensors are used to measure the desiccant mass flows at each tank outlet.

$\chi_{d(in)}$ and $\chi_{d(out)}$ differs, the mass flow of the desiccant water solutions $\dot{m}_{s(in)}$ and $\dot{m}_{s(out)}$ also differs.

In the beginning the system was designed and tested with shovel wheel pumps on all sides of the absorber. Displacement pumps would have been the preferred option, however they typically don't come flow adjustable and are not meant for continuous use. The shovel wheel pumps worked fine when testing with water, however they cannot handle the more viscous desiccant. Also the shovel wheel pump at the absorber back flow gets stuck occasionally at temperatures below 0 °C, which is why all of the pumps except the one at the backflow of the absorber were later replaced by gear pumps.

3.5 Hydraulic system

In order to supply both the absorber and the air coolers with cold water and the regenerator with hot water, a hydraulic system was build (Fig. 14). The tempering system consists of two separate cycles. A water heater connects to the regenerator and two bath thermostats are used to cool the absorber and both air coolers. The hot cycle consists of a single pump group and is pressurized slightly below 3 bar. Because the closed system is pressurized, it is connected to an expansion vessel. The water heater is capable of reaching up to 60 °C and is filled with tap water. The cold cycle consists of two bath thermostats, three pump groups and a hydraulic separator to avoid pumps working against each other, as the bath thermostats have their own pumps. The two thermostats are connected in series with the smaller one feeding into the bigger one.

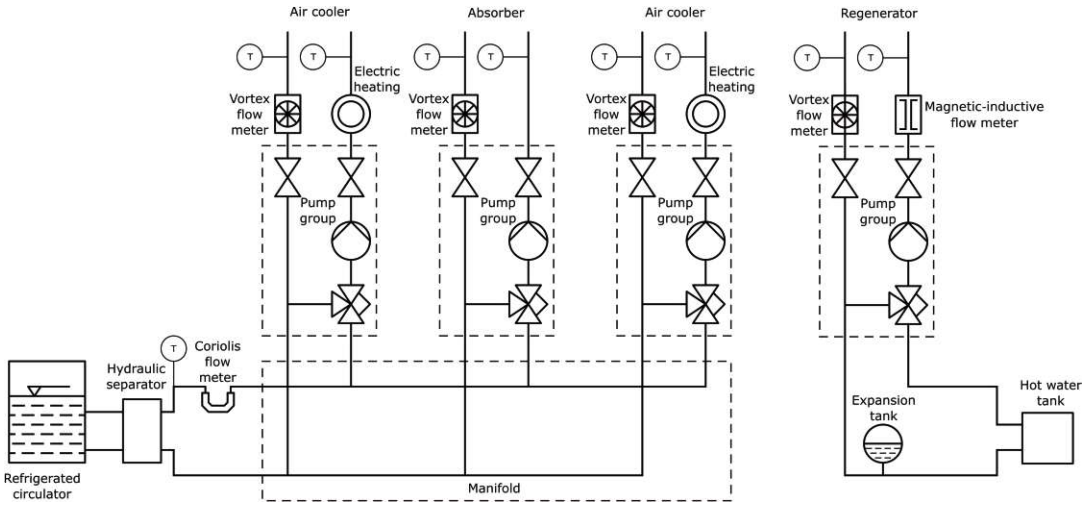

Figure 14: The hydraulic system consists of a cooling cycle connected to the air coolers and the absorber and a heating cycle connected to the regenerator. Temperature sensors (T) are positioned right at the inlet and outlet of the air coolers and falling film absorbers. The volumetric flow through each is measured using a vortex flow sensor. An additional Coriolis flow sensor is used on the clod side for calibration and calculating the total cooling power. On the hot side a magnetic inductive flow sensor is used to validate the results of the vortex flow sensors.

3.5.1 Pump groups

The ESBE GRF111 pump groups consist of three pipes forming an H. One of the junctions is open. The other contains a ESBE ARA639 mixing valve, used to regulate the mixture of the liquid. Fully opening the valves results in all the liquid moving out at the top coming from the inlet at the bottom. Fully closing the valve results in no liquid being added from the bottom, essentially forming a closed loop, where all the liquid coming out of the top valve moving through the return flow H-connection. The valve can be operated manually or remotely. On top of the mixing valve a Wilo Yonos Pico 25/1-6 180 circulation pump drives each cycle. These pumps cannot be operated remotely so the heat transfer is regulated by adjusting the mixing valve, which is also more precise than controlling the pump throughput. The tree pump groups on the cold side are mounted on top of the ESSBA GMA431 manifold.

As these pumps can have problems with cavitation the hot cycle is pressurized to about 3 bar. The cycle on the cold side has three pump groups connecting to the air coolers and the absorber, as seen in 14. The cold cycle can not be pressurized, as it is connected to an open bath thermostat. However the low temperature and the addition of antifreeze lowered the vapor pressure enough to prevent cavitation at lower performances. The hot cycle connects to an expansion vessel in order to retain the pressure.

Above each of the pump groups a safety group is mounted. They consist of three parts: A barometer, a quick vent and an over pressure valve. The quick vent consists of a basic valve, which is closed by a ball. If the ball is emerged in water, it floats, closing the valve. If it is surrounded by air, it can sink, letting the air escape. The safety valve is closed by a spring. At a pressure of 3 bar, the spring force is no longer strong enough to withstand the water pressure and opens until the pressure is reduced to below 3 bar.

3.5.2 Hydraulic separator

The three pump groups on the cold side are connected in parallel by a distribution bar. The parallel arrangement allows each pump group to draw a different amount of coolant from the bath thermostats. There is a small influence on the other groups, since the current draw slightly influences the input pressure of the others. This effect was taken into account for the design of the control system, but in general, each pump can be operated without considering the state of the others.

Connecting the distribution bar directly to the bath thermostat however would lead to some issues. The distribution bar with the three pumps in parallel can essentially be considered as one single pump, with the throughput of all three pumps combined. The bath thermostat has its own inbuilt pump, which has to be active when using the

system. The combination of the 3 pump groups would then be connected in series with the pump of the bath thermostat. This could cause problems if the pumps try to achieve different flow rates. To relieve any pressure created by the two sides, a DN25 hydraulic separator was installed between them. A hydraulic separator consists of a single piece with 2 connections on each side. One side connects to the thermostat, the other to the distribution bar. On the top a quick vent is mounted and on the bottom a small ball valve can be used for filling and emptying.

3.5.3 Bath thermostats

The Julabo FP55-SL was the most powerful bath thermostat available to use for the test rig. However it alone did not provide enough cooling performance to power both air coolers and the absorber. Therefore, a smaller Julabo FP51-SL was installed in series with the first one (Fig. 15). Both thermostats have their separate inlet and outlet pumps. Simply connecting the input and output hoses to the bath of the first thermostat would lead to some problems, as it can not be assumed that both pumps generate the same amount of throughput. Just a tiny difference could result in one bath fully emptying into the other. To prevent this from happening, the bath thermostats were positioned in a way, where both coolant levels are at the same height. To correct for any differences, resulting from pumping, three connection hoses where installed. Each connects the two baths and is filled with coolant. When a level difference builds up, the different height levels will result in a balancing current in the hoses. In theory one hose would be enough, however at any point a hose might fail due to air bubbles building up, destroying the coolant bridge. The baths are typically closed after filling to prevent unwanted particles from entering the system. As the standard lids could not be used without removing the connection hoses, special lids with cut outs for the hoses where 3D-printed.

3.5.4 Filling and emptying

There are 6 ball valves in total used for filing and emptying, 4 on the cooling cycle and 2 on the heating cycle. Each of them can be connected to a hose via a Gk-clutch. One valve is mounted beneath each heat exchanger and falling film absorber, one at the hydraulic separator and one next to the expansion vessel. The valves at the heat exchangers and falling film absorbers are only used to drain any remaining liquids when emptying. Filling the cycles was done quite different for the cooling and the heating sections. On the hot side the system was filled trough the bottom valve while running the circulation pump in partial operation until the system was free of air. The pressure was set to slightly below 3 bar, which is typical for commercial heating systems. As the cold side is connected to an open bath thermostat, it was not possible to fill the system the same way, as the thermostat pumps are not able to seal the cooling cycle from the cooling reservoir. It

Figure 15: The main Julabo FP55-SL bath thermostat on the right was supported by the smaller Julabo FP51-SL on the left. The internal coolant heights are being leveled by the three connection hoses.

was therefore filled using the thermostat pumps, while continuously filling the thermostat tank as it emptied into the system. To test for leakages the system was first fully filled with water. After successfully testing, the water was drained again and the system was filled with a water and ethylene glycol mixture. The mixture has a freezing point of -15 °C, which was tested using a hand held refractometer and cross checked with the density measurement of the Coriolis and a nearby temperature sensor. In the test rig setup, the majority of the cooling cycle is positioned higher than the thermostat level. To avoid the coolant from flowing back while the pups are not running, a magnetic valve closes the connection to the bath as soon as the bath thermostat is turned off.

3.6 Sensors and calibration

In order to measure the effectiveness of the system, regulate the actors and implement important safety features, multiple sensors are positioned all over the test rig. Temperature and flow rate sensors are used to calculate the energy transfer at each falling film absorber and give feedback for the regulation of the heating registers and air coolers for air conditioning. Humidity sensors measure the effectiveness of the absorber and regenerator. Differential pressure sensors are used to measure the pressure drop over the absorber and regenerator, while the air speed is measured by a hot wire anemometer. Tank level sensors and liquid sensors provide important safety information.

3.6.1 Temperature sensors

All temperature sensors used on the test rig are PT100 class A resistance thermostats with a rigid protection tube. They work by measuring the temperature dependant resistance of a wire. Though the temperature dependence of the resistance is a complicated function, at temperatures between -20 °C and 100 °C a linear approach results in a decent fit. They are called PT100, because they have a standard Resistance of 100 Ω and are made out of Platinum. The standard calibration table is derived from a polynomial function of fourth degree:

$$R(T) = R(0)(1 + At + Bt^2 + C[T - 100]T^3) \tag{5}$$

$$A = 3,90802 \cdot 10^{-3} C^{-1}$$

$$B = -5,802 \cdot 10^{-7} C^{-2}$$

$$C = -4,2735 \cdot 10^{-12} C^{-4}$$

The resistance at each temperature R(T) is determined by the resistance at 0 °C $R(0)$ and a polynomial function with coefficients A, B and C depending on the material used for the wire. Taking the data from the standard table might still lead to errors resulting from poor calibration by the manufacture. In order to ensure the temperature sensors are calibrated with minimal discrepancies, at least between each other, all sensors where compared to a an externally verifiable calibrated reference sensor and calibrated to that. This was done by putting both the refference sensor and a sensor to be calibrated into a shared water bath, where they sat for 10 minutes. All sensors were compared at 11 different temperatures ranging form -20 °C to 80 °C. Most sensors matched the standard very well, but some deviated by more than 1 °C resulting them being replaced. Resistance is typically measured using Ohms Law:

$$R = U/I \tag{6}$$

Either voltage U is applied to the resistance R and the current I is measured or the other way around. As the resistance has to be measured as precisely as possible, just

connecting a cable to each end of the platinum wire and measuring the resistance of the system, will not suffice. This is because the cable resistance adds to the resistance of the platinum wire as seen in Fig. 16:

$$R_{tot} = R_{w1} + R_{w2} + R_{PT100} \tag{7}$$

The total resistance R_{tot} measured in this configuration is the resistance of the sensor R_{PT100} with the addition of the wire resistances R_{w1} and R_{w2}. This additional error increases with cable length. To circumvent the problem of the additional cable resistance there are two alternative ways of wiring a Pt100 sensor. One is to use a third cable connected to one side of the resistor as seen in Fig. 17. A constant current is applied through the resistor via wire 1 and 3. The voltage is measured between wire 2 and 3 as well as 1 and 2. As no current flows through wire 2, the voltage drop can be neglected:

$$U_{w2-w3}/I = (R_{PT100} + R_w) \tag{8}$$

U_{w2-w3} is the voltage measured between wire two and wire 3. In this setup the wires are all assumed to have the same resistance R_w. The resistance of wire 1 can then be calculated, by measuring the voltage between wire 1 and 2:

$$R_w = U_{w1-w2}/I \tag{9}$$

U_{w1-w2} is the voltage measured between wire 1 and 2. Since almost no current flows through wire 2 due to the high internal resistance of the volt meter, the resistance of a single wire can be calculated.

In most cases it is accurate enough to assume that the two wires 1 and 3 have the same resistance. This is not necessarily required by wire 2 as the current through it can be neglected. Resistance of the sensor can than be calculated by subtracting the wire resistance from the resistance measured between wire 2 and 3:

$$R_{PT100} = (R_{PT100} + R_w) - R_w = \frac{U_{w2-w3} - U_{w1-w2}}{I} \tag{10}$$

The three wire method is mostly sufficient to compensate for the wire resistance as the difference in wire resistance usually doesn't result in an error large enough to contribute in a meaningfully way compared to the sensitivity of the sensor. However, with increasing wire length it still might become a consideration and there is a way of avoiding this problem entirely using a fourth wire. In this case 2 wires are connected on each side, as seen in Fig. 18. A constant current is applied between wire 1 and 4 while the voltage is measured between wire 2 and 3:

$$R_{PT100} = Uw2 - w3/I \tag{11}$$

Since almost no current moves through wire 2 and 3 the wire voltage drop can be neglected. For this test rig only 4 wire arrangements were used.

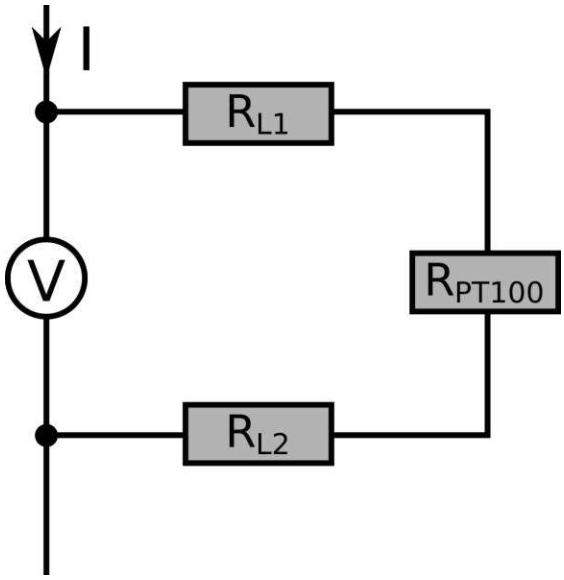

Figure 16: The 2 wire system is prone to errors, as the wire resistance is added to the resistance of the platinum wire.

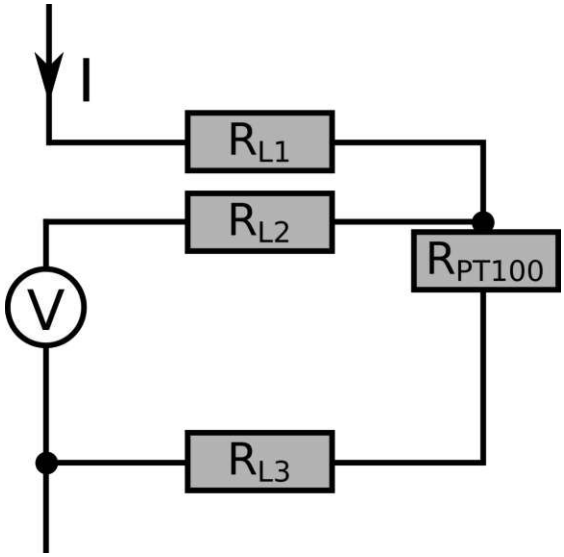

Figure 17: In the three wire system, the wire resistance can be measured between wire 1 and 2. To calculate the resistance of the sensor, it has to be assumed, that wire 1 and 3 have the same resistance.

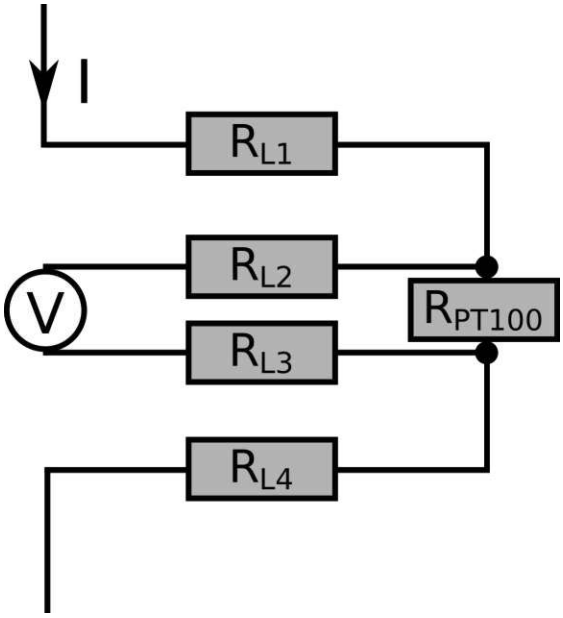

Figure 18: The 4 wire system gives accurate results, even with varying wire resistances.

Most of the Pt100 sensors where inserted into the ducts and the pipes through compression fittings. In case of the air ducts, holes where drilled into the ducts and the fittings where screwed in (Fig. 19). They where then sealed using silicone. The only exception to this are the sensors mounted between the two filters. The measurement should be done as close to the absorber as possible, however the sensors are unable to reach the center of the duct through a compression fitting, as the duct is at its maximum diameter here. In order to reach the center, the sensors where directly mounted to the wire grid of the large HEPA-filter using zip ties as seen in Fig. 20.

3.6.2 Humidity sensors

There are multiple different ways of measuring air humidity ranging from the lengthening of human hair to the absorption coefficient of certain wavelength of light of the air. Many common modern sensors measure either the resistance or dielectric constant of a hygroscopic layer. In the test rig all of the EE08 humidity sensors use the capacitive method. They consist of a capacitor with a hygroscopic layer in between. The sensor is connected to a small measuring transmitter, which is converting the measured capacitance into a humidity value which is then transferred as a 4-20 mA signal. The sensor is mounted inside a fine stainless steel mesh lid. Alongside the humidity sensor a class A PT100 element is mounted inside. It is positioned only a few millimeters away from the humidity sensor. With the sensors so close together spatial divergence can be neglected. This makes it possible to calculate other parameters like the dew point and absolute water

Figure 19: The inside of the air duct with a humidity sensor on the left and three temperature sensors on the right.

content in the air. The measuring transmitter gives of a small amount of heat, resulting in a temperature increase inside the stainless steel lid of about 1-2 °C. For this reason they alone cannot be used to calculate performance of the heat exchangers, because they don't measure the air properties inside the duct. The calculations of the dew point and absolute water content are still accurate for the air outside the humidity sensor, as they are independent for isobaric heating. In order to calculate the relative humidity and vapor pressure inside the air duct, the temperature measurements of additional PT100 sensors mounted close to the humidity sensors were used alongside the absolute water content measured inside the humidity sensor.

The humidity sensors came calibrated out of the box. After a few months of testing the absorption cycle they started miss aligning, reporting a difference in humidity of about 7 % between the highest deviating sensors. The manufacturer stated that these deviations from the calibration can happen if the sensors remain in a humid environment for an extended period of time. In order to recalibrate them, they were first cleaned inside an ultrasonic bath in isopropanol and then in deionized water. They were then mounted on top of the fine HEPA-filter in the absorption section together using an externally verifiable calibrated humidity sensor, to ensure equal conditions for all of them (Fig. 20).

3.6.3 Pressure sensors

The two Huba Control Typ 699 differential pressure sensors over the absorber and regenerator are used to measure the pressure drop for different amounts of desiccant flow rate. They work by having the two sides connected to a chamber each with a diaphragm in between. The diaphragm is connected to a piezo electric crystal, which translates the force into voltage. In order to minimize the contribution of dynamic effects inside the duct to the measurement, 4 tubes are connected to the air duct on each side of the falling film absorber. They reach about 5 cm into the duct. The four tubes are then joined by T-connectors and lead into one chamber of the differential pressure sensor. The small pressure changes inside the air duct can easily be picked up by differential pressure sensors. They are however not large enough to significantly change the properties of the air. The pressure changes of the atmosphere on the other hand are. For this reason, a Comet T2114 barometer was installed next to the test rig.

3.6.4 Coriolis sensors

In order to properly determine the performance of the falling film absorbers, the flow rate of coolant and hot water has to be measured precisely. To accomplish this, three different types of sensors where put in place. They vary in price and precision. The

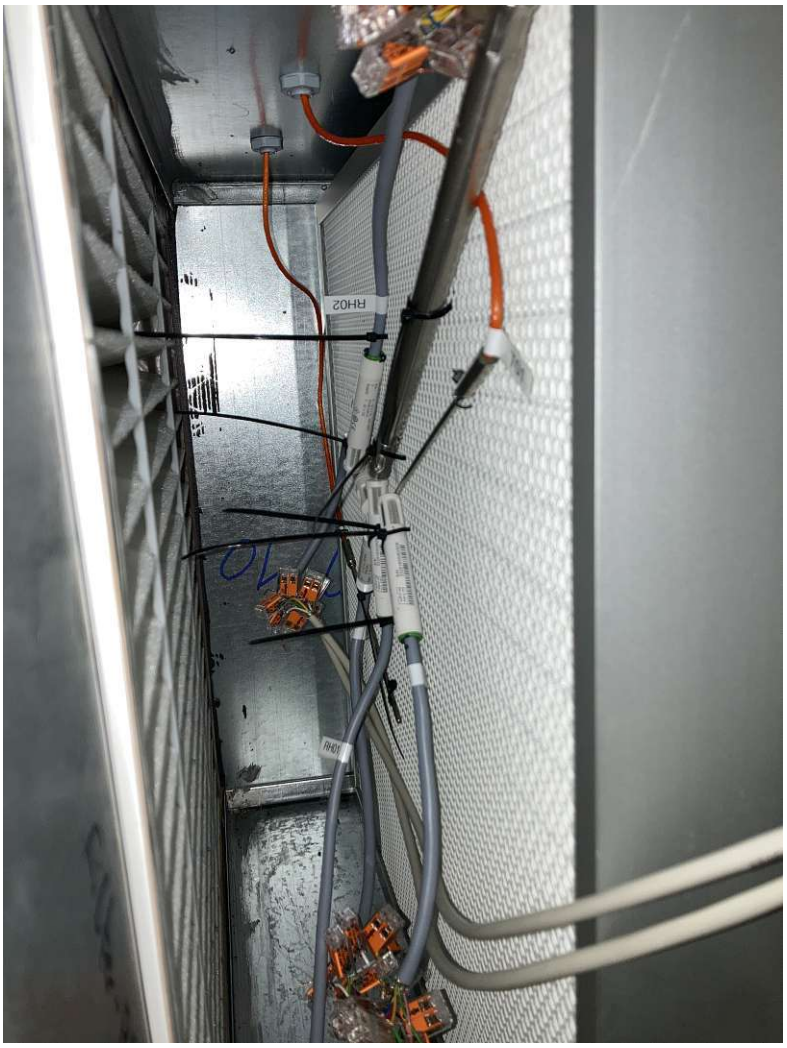

Figure 20: In order to callibrate the humidity sensors, they were mounted on the HEPA-filter using zip ties. The larger one in the middle provides the reference for calibration.

most accurate and expensive sensors used are Coriolis flow sensors. There are 4 smaller CMF010M Coriolis sensors in the desiccant cycle and a large CMF025M sensor at the exit of the Julabo. They are complimented by cheaper vortex flow sensors and magnetic flux sensors. The Coriolis sensors work, as the name suggests, by taking advantage of the Coriolis effect. The incoming liquid is split into two thin tubes which are arranged in a triangular formation. The tubes are then driven to vibrate vertically to the flow of the liquid towards and away from each other. The frequency of the tubes correlates with the mass of the liquid inside. Assuming the tube is fully filled with liquid(l) with no bubbles inside, its density can be calculated from the frequency measurement:

$$\omega = \frac{1}{2\pi}\sqrt{\frac{k}{m}} \tag{12}$$

$$m = \rho_l V_l + m_{tube} \tag{13}$$

The natural frequency ω of the vibrating tube depends on the spring constant k and the total mass m. This mass depends on the mass of the tube m_{tube} and the mass of the liquid, which depends on the volume of the liquid inside the tube V_{liquid} and the density of the liquid ρ_{liqud}. As liquid is flowing through the vibrating tube, the down stream part experiences a delay due to the Coriolis effect. The resulting phase shift increases with higher current and can therefore be used to calculate the mass flow. A 4-20 mA signal is used to transmit the mass flow measurement. On top of this analog constant voltage, the density information is transmitted as a highway addressable remote transducer (HART) signal. A HART signal works by shifting between modulating a 1.2 kHz and a 2.2 kHz waveform on top of the comparably low frequency 4-20 mA analog signal. The density information in this test rig is especially important for the desiccant water solution, as it can be used alongside the temperature information to calculate the water concentration. For this reason 4 Coriolis are used to measure the mass flow through each desiccant pump. One additional Coriolis is installed in the cooling cycle of the tempering system. All the Coriolis were calibrated by a reference Coriolis. To do this, each one was hooked in series to the calibrated Coriolis in a closed loop system and the flow rate was adjusted.

3.6.5 Vortex flow sensors

In addition to the five Coriolis, four Huba Control Typ 210 vortex flow sensors are used to measure the flow rate through each heat exchanger and falling film absorber. When a cylinder is inserted into a current, a periodical vortex street emerges downstream of that cylinder (Heinze et al.). The vortex sensors operate by inserting a disturbance body into the pipe and measuring the frequency of the resulting vortex street (Fig. 21). They come calibrated for water and had correction tables for more other liquids, but not for the ethylene glycol solution in use. The calibration tables are needed, as the frequency

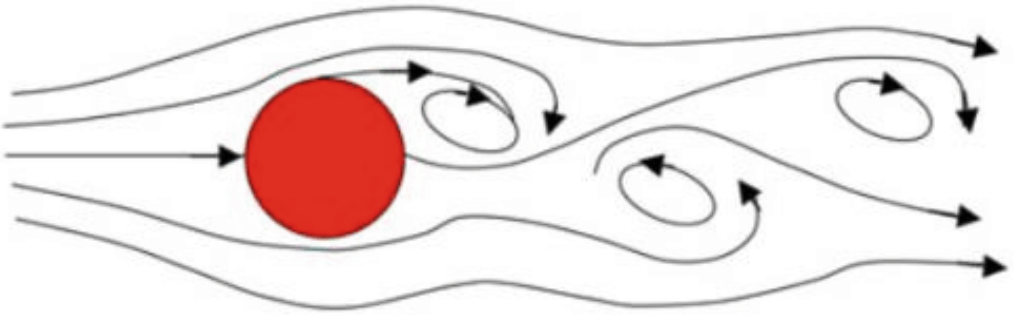

Figure 21: A typical formation of a vortex street, taken from (Heinze et al.). The oscillation period depends on the speed of the fluid.

of the vortex street depends on the properties of the liquid:

$$f = Sr\frac{v}{d} \tag{14}$$

The frequency of the vortex street depends on the fluid velocity v, the characteristic dimension of the body d and the Strouhal number Sr, which has a complicated dependency on the Reynolds number.

$$Re = \frac{\rho\, v\, L}{\eta} \tag{15}$$

The Reynolds number in turn depends on the density ρ and dynamic viscosity η of the liquid, as well as a characteristic length L. The dependency on viscosity meant not only that the out of the box calibration is useless for the ethylene glycol water solution, but also, that each sensor had to be tested at different temperatures, as the viscosity depends on it.

In order to calibrate each vortex flow sensor on the cooling cycle, one of the mixing valves was fully open, while the other two where fully closed. This results in all the coolant flowing through the Coriolis flow sensor downstream of the bath thermostats to be forced through one of the vortex flow sensors. The measurements where done for multiple temperatures and flow rates. The vortex flow sensor on the hot side uses the calibration done by the manufacturer, but a more precise magnetic flux flow sensor was installed in series to determine it's performance.

3.6.6 Magnetic flux flow sensor

Even though the vortex flow senor in the heating cycle measures the volume flow rate of water, a Rosemount 8700 magnetic flux flow sensor was added in series to validate

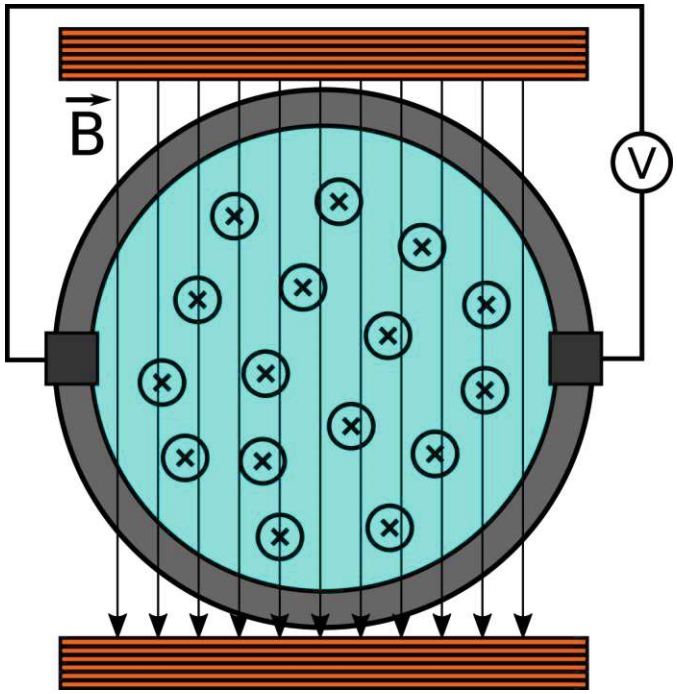

Figure 22: The magnetic flux flow sensor is based on the Lorenz force. By applying a magnetic field vertically to the flow direction of the liquid, charge carriers are pushed to the sides of the pipe, where the resulting voltage can be picked through electrodes. As the Lorenz force depends on the speed of the liquid, the volumetric flow can be calculated. In order to avoid errors resulting from static build up, the magnetic field direction is switched periodically, so electromagnets have to be used instead of permanent magnets.

its results. The mass flow sensor is based on the principal of induction (Fig. 22). It operates by creating a magnetic field perpendicular to the axis of flow. Charge carriers in the liquid are then pushed to the sides of the pipe by the Lorenz force, resulting in a voltage between the two sides:

$$\vec{F}_{\mathrm{L}} = q \cdot \left(\vec{v} \times \vec{B} \right) \tag{16}$$

The Lorenz force $\vec{F}_{\mathrm{L}}$ acting on a particle of charge q is proportional to the cross product of the speed $\vec{v}$ of the particle and the magnetic field strength $\vec{B}$ at its location. The voltage resulting from the Lorenz force is therefore proportional to the flow rate. This sensor was calibrated similar to the other Coriolis sensors, by installing it with a reference sensor in series.

3.6.7 Hot wire anemometers

In order to properly account for the energy transfer in the heat exchangers and the falling film absorbers it is important to not only measure the mass flow rate of the tempering liquid and the desiccant but also the mass flow rate of the air. There are multiple techniques for measuring air velocity. For this application the EE650 hot wire anemometers were chosen. They work by measuring the thermal losses of a hot wire suspended in the air duct. This method comes with a problem: The anemometer only measures the air velocity at one point in the air duct. The air speed in the duct can however by no means be expected to be constant throughout the duct. The anemometer is positioned downstream of a flow straightener and has over 7 pipe diameters of straight entrance length. The flow was at first assumed to be laminar inside the circular pipe, which results in a paraboloid shaped flow profile, as shown in Fig. 23. The airspeed at the pipe wall is 0 and has a maximum at the middle. The average air speed would then be equal to half the speed measured in the middle of the pipe:

$$v(x) = v_0 \left(1 - \frac{x^2}{R^2}\right) \tag{17}$$

$$\bar{v} = \frac{1}{R^2\pi} \int_0^{2\pi} \int_0^R x v(x) dx \tag{18}$$

$$\frac{1}{R^2\pi} 2\pi v_0 \int_0^R x - \frac{-x^3}{R^2} dx = \frac{2}{R^2} \left(\frac{R^2}{2} - \frac{R^4}{4R^2}\right) = \frac{1}{2} v_0 = \bar{v} \tag{19}$$

In the paraboloid shape distribution the air speed at each point into the direction of the pipe $v(x)$ is equal to the speed in the center $v(x)$ multiplied by a paraboloid with the maximum of 1 in the center of the pipe and that is 0 when die distance from the center x is equal to the radius of the pipe R.

The anemometer is mounted to the air duct so that its depth can be altered. The wire of the anemometer is mounted in the center of a flat plane, which can be rotated by rotating the anemometer. Since the rotation and altering the depth of the hot wire both alter the results of the measurement, the positioning needed to be done extremely precisely, in order to accurately measure the speed in the center. After measuring the speed contribution along the vertical axis of the air duct however, we noticed that for our setup the paraboloid isn't a good enough approximation and thus positioning of the wire inside the duct is not as important. We therefore calibrated the mass flow rate through the air duct specifically for our setup.

In order to do this, the mass flow rate of the air was calculated by measuring the heat flow rate of the coolant to the air and the temperature difference resulting from it. The air and coolant temperature through the air cooler and the coolant flow rate can be measured. To reduce thermal losses to the environment, the temperature in the duct

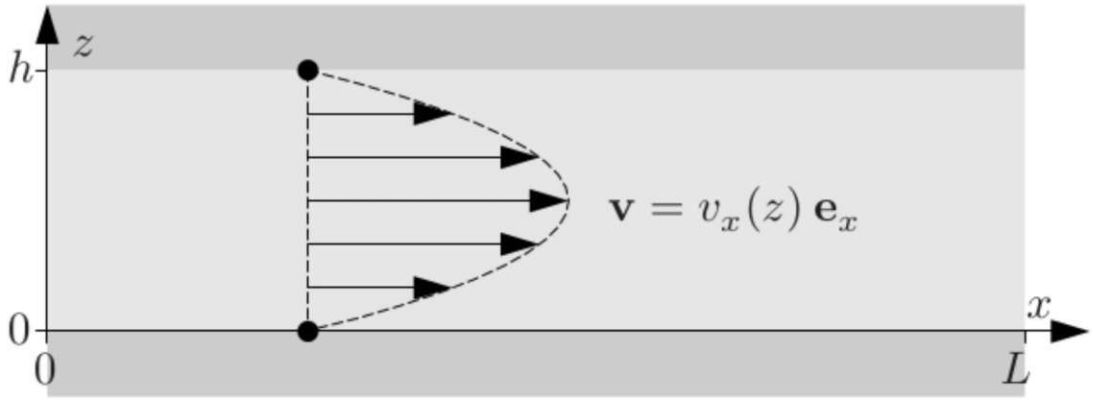

Figure 23: The flow velocity inside a cylindrical pipe of laminar flow taken from (4).

was set to be close to room temperature. The air was cooled down by about 3 °C below room temperature at the exit of the air cooler and further downstream heated up by the heating register to about 3 °C above room temperature. This gives a spread of about 6 °C. This symmetric approach was chosen since the higher the temperature spread of the air and the coolant, the lower the relative effect of measuring errors. At the same time the difference to the surrounding should be as low as possible in order to reduce losses to the environment. Since the vortex flow sensors were not calibrated for this temperature range, two of them where closed completely and one remained fully opened. This forces all the coolant to move through the Coriolis flow sensor into the heat exchanger, making it possible to use the accurate Coriolis measurement for the mass flow rate. The heat capacity of the ethylene glycol water solution (l) and of air (a) can then be used to calculate the mass flow rate of the air:

$$\dot{Q}_a = -\dot{Q}_l \tag{20}$$

$$c_a \dot{m}_a \Delta T_a = -c_l \dot{m}_l \Delta T_l \tag{21}$$

$$\dot{m}_a = -\frac{c_l \Delta T_l}{c_a \Delta T_a} \dot{m}_l \tag{22}$$

The specific heat capacities c are assumed to be constant over the small temperature ranges. The heat exchange rate $\dot{Q}$ between the air and the liquid is equal to the heat capacity multiplied by the mass flow $\dot{m}$ and the temperature ΔT difference of the medium.

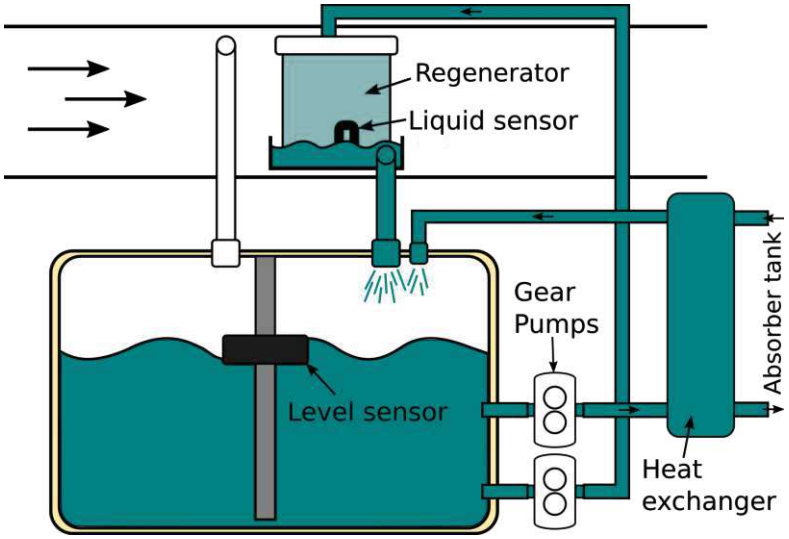

Figure 24: Each desiccant tank has an outlet connected to the heat exchanger connecting to the other desiccant tank and one connected to the absorber/regenerator. The two inlets are connected to the top of the tank. The additional (here white) tubing attached to the air duct prevents over pressurization of the tanks.

3.6.8 Tank level sensors

Measuring the tank levels is an important safety measure. Since the system is designed to have the two desiccant pumps continuously cycling the desiccant water solution (s) back and forth, a net difference in flow rate of the desiccant (d) is unavoidable. In order for the system to be stationary the desiccant transfer m_d would have to be the same in both directions:

$$\dot{m}_{d(in)} = \dot{m}_{d(out)} \tag{23}$$

However, the water concentration in both tanks is not the same and the desiccant ratio $x_{s(out)}$ can only roughly be estimated using the density and temperature of the mixture.

$$x_{s(in)}\dot{m}_{s(in)} = x_{s(out)}\dot{m}_{s(out)} \tag{24}$$

There is no risk of pressure building up in one tank, since they are directly connected to the air duct, but fully emptying one tank would result in the pumps of the other tank running dry.

Therefore a simple level sensor was installed in both tanks, as seen in Fig. 24. It consists of a swimming ring containing magnets, which can move along a metal cylinder mounted vertically in the tank. The cylinder has hall sensors mounted inside, making it possible to differentiate between 5 different fill levels of the tank.

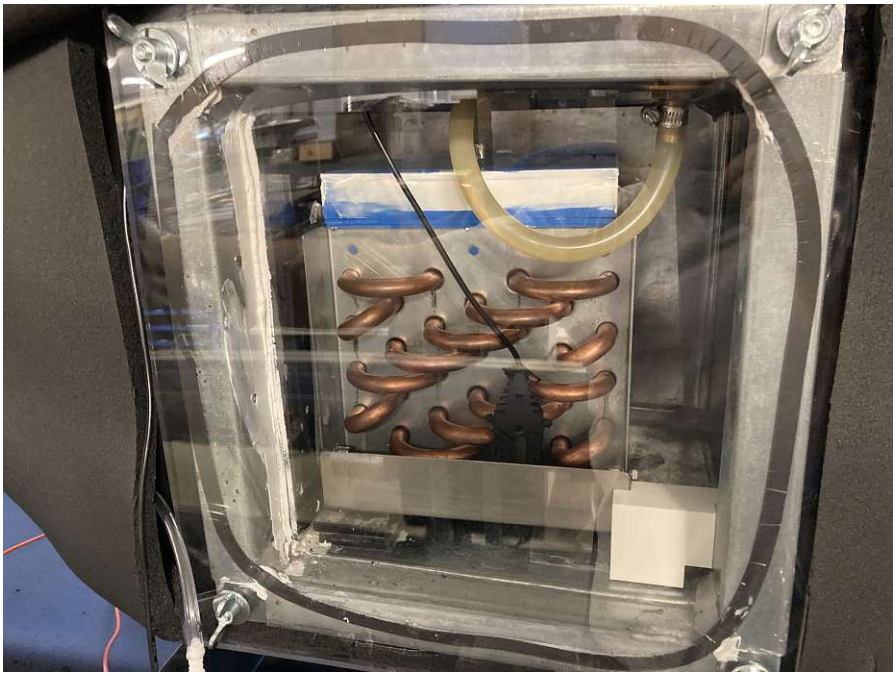

Figure 25: The regenerator is pushed against the acrylic glass window on the left by the white 3D-printed part at the bottom right. The black liquid sensor has two exposed contacts at the top of the drip tray. If the resistance between these contacts reaches below an adjustable level, the power of the desiccant supply gear pump is cut.

3.6.9 Leakage sensors

Leakage of the desiccant at any point has to be avoided. This was one of the main challenges using it in combination with a falling film absorber. Even if the system is properly sealed, there are still two ways for the desiccant to escape into the air ducts. One is "carry over" into the air. To account for this, the 3D printed inserts don't reach all the way to the back of the falling film absorbers and the two filters catch the desiccant aerosols.

The other, and more serious one, is the spillage of the drip tray. The reason for a spillage might be the complete blockade of the back flow pipe (for example due to malfunction of the shovel wheel pump at the absorber). Even if the inflow is slightly higher than the back flow, the gear pumps might completely empty one tank into the air duct within minutes. To address this a H-Tronic WPS 4000 liquid sensor was installed at the top of each tray, shutting down the gear pumps as soon as it triggers (Fig. 25). They work by measuring the resistance of an open circuit, with two exposed points. Once these points are connected by a liquid, the resistance drops, activating the sensor. Conveniently the

cut off resistance can be altered, adapting to the liquid used and the temperature. In our case the desiccant has a higher resistance than water, especially at low temperatures.

3.7 Actors and control

In order to operate the test rig, all the sensors and actors where connected to an APROL system of B&R Industrial Automation GmbH. All the data acquisition and control was realized through this system, which made it possible to operate the rig fully remotely. With very few exceptions listed below, all the regulation was done through PID controllers. A PID controller a common way to regulate variable output signals. It consists of a proportional response (P), adjusting the control value only considering the difference to the target value, an integral response (I), adjusting for the accumulated difference to the target value in the past and a differential response (D), depending on the rate of change of the control value:

$$y(t) = K_p(x - w) + \frac{1}{T_i}\int_0^t (x(\tau) - w)d\tau + T_d\frac{d}{dt}(x(t) - w) \tag{25}$$

The control parameter $y(t)$ depends on a proportional factor Kp multiplied by the difference in the measured process variable x and the desired set point w as well as an integral and a differential component with the adjustable coefficients T_i and T_d respectively. As the purpose of this test rig is to only measure the system in stationary operation, the differential coefficient was mostly set to very low values in order to simplify the process of setting the control parameters. The fact that the control parameters were not optimized was not a problem as the time of stabilizing the system is comparatively small to running an experiment. Also some of the control values are dependent on multiple different actors and some have some significant latency. The controls where therefor chosen to reduce the risk of unwanted interference between different actors. In the desiccant system the 4 gear pumps can be controlled to adjust the flow through the four outlets. Conditioning of the air on the absorption and regeneration side is done differently as water has to be introduced in the absorption side and removed in the regeneration side. For the absorption cycle, water is introduced by both a steam lance and an ultrasonic humidifier. The steam lance can be controlled through the control system while the ultrasonic humidifier can only be adjusted manually between four settings. The temperature is controlled by the air cooler and the heating register. The air cooler can be defrosted by heating the incoming the glycol water solution using a heat rod. On the regeneration side, the humidity is controlled by the air cooler, while a heating register adjusts the temperature. The two fans on the absorption and regeneration cycle can be regulated, while the one for the fume hood can only be turned on or off.

Two control cabinets are positioned at the front of the test rig. The left one houses a a fuse switch connected to every actor and sensor in the rig that needs high voltage supply. This makes it possible to disconnect each device from the AC supply separately without having to shut down the entire system. The left control cabinet also houses two 24 V power supplies. One is used to power the actors and the other to power the control system. The cabinet on the right houses all the logic and controls and is only powered

by the 24 V power supply.

3.7.1 Desiccant pumps

The gear pumps used to transfer the desiccant are MGD2000 brushless micropumps from RS PRO. The only exception is the M510 brushless paddle wheel pump used at the outlet at the absorber, which is set to a constant power output. The gear pumps get their feedback from the Coriolis flow sensors. The flow rate to the absorber and regenerator can be adjusted, simply by changing their target value in the control system. While the pumps are able to adapt with almost no latency, the control parameters are chosen to have the adjustments in output value act slow enough to prevent overpressurization. These gear pumps are able to create pressure differences easily large enough to destroy the latex hoses. If the pumps would immediately adjust their throughput when changing the target value, the inertia of the viscous desiccant delays the flow increase further down the cycle, resulting in a pressure increase forcing the hose to expand. The exchange rate between the two tanks depends on the flow rate measured by the Coriolis flow sensors as well as the height of the tank levels. The tank levels in both tanks can rise and sink by more than one level by turning on the absorber and regenerator, as the drip tray, distributor and hoses get filled. The goal for most operations is to keep the desiccant tanks at roughly the same level. To accomplish this, one of the target values for the throughput can be set manually, while the other will be set to 15 % higher or lower, dependent on which level is higher. That way the difference in flow rate never exceeds 15 %, while ensuring continuous flow in both directions. The threshold of 15 % proved to be enough to account for the density differences resulting from the water concentration and temperature not being equal. This method results in a hysteresis-like behavior as the time of the tank level changes differ vastly dependent on the other settings on the rig.

3.7.2 Steam humidifier

To adjust the humidity in the absorption side, a Carel heaterSteam 4 humidifier is used alongside an ultrasonic humidifier. The steam humidifier has the advantage of giving very precise control over the amount of water that's being added to the system. It is even capable of adding enough water to the air on its own, however it has the downside of adding it as steam at very high temperatures. This introduces a lot of unwanted heat, which in combination with the heat losses to the outside can overwhelm the air cooler. To reduce the heat added through the steam humidifier, while still having a controllable humidity, an ultrasonic humidifier was added to the system. To accomplish a proper seal to the curved pipes, the adapters for it and the steam humidifier where all 3D-printed. The humidifier is not capable of receiving external control signals and

only has four output settings which have to be set manually. To operate the test rig in most applications, the ultrasonic humidifier is set to its maximum output so that the system nearly reaches the desired humidity level and the steam humidifier controls the remaining difference. The humidity control of the steam humidifier uses the humidity sensor in front of the absorber as the feedback value. It's controlled using a 4-20 mA signal. As the water of both the ultrasonic and the steam humidifier gets combined with the cold air in the duct, a lot of fallout is produced. Small droplets condense on the sidewalls and run to the bottom of the air duct. To get rid of this unwanted water, the air duct in this section was installed sightly angled downwards in respect to the air flow direction. A bent steel plate mounted in the air duct collects the incoming water and funnels it into a hose connected to the bottom of the duct. This hose is then connected to a canister as the amount of water leaving the system is very small, however it is important that it is connected in a way where it forms a siphon, to seal the inside of the duct and prevent air exchange.

3.7.3 Hydraulics

There are four ways to influence the heat flow through the heat exchangers. The bath thermostat temperature can be altered, the bath thermostat pumps can be adjusted, the mixing valves can be set, and the centrifugal pumps can be set to different speeds. The bath thermostat pumps are only adjustable to 4 different settings and are always set to the maximum value, in order to maximize the pre-pressure of the centrifugal pumps. This increases the maximum pump performance, before cavitation occurs. The centrifugal pumps are not adjustable remotely, so they are set to a value as high as possible where cavitation won't occur and the vortex sensors still are still operating in the calibrated range. As the bath thermostat temperature can only respond slowly, compared to the mixing valves and the system is struggling to provide enough cooling to overcome all the heat losses, the thermostat temperature is set to slightly below the supply temperature to maximize cooling performance but above -15 °C so the glycol water solution doesn't freeze in case no power is drawn. All the air ducts and cooling pipes are covered in insulation materials, however the heat losses can not be neglected, as the area and temperature differences are so large. Controlling the temperature of the heat exchangers, the absorber and the regenerator is done by controlling the mixture of back flowing liquid and moderated liquid through the mixing valves in the pump groups. While the power of each pump can only be adjusted manually, the mixing valves can be operated by a 4-20 mA input signal. In case of a malfunction, they can be set manually.

The feedback values for the absorber, regenerator and the air cooler in the absorption cycle are the respective inlet temperatures. Compared to using the air temperature, this has the benefit of a enabling a faster approach to the set value. The air cooler on the regeneration cycle gets its feedback from the humidity sensor in front of the regenerator. The reason for this is, that the air cooler is used to control the humidity of the incoming

air through condensation. Setting the temperatures of the air is done with the two air heaters.

The control values for the mixing valve on the heating side were chosen to achieve a fast approach to the set value. In the cooling system the flow rates through the heat exchangers depend on the settings of the other valves, as they influence the pre-pressure of the pumps. This can lead to some unwanted vibrations caused by this interference. To address this issue, the control parameters were set so that the response speed of the three valves differs by over a factor of two. The faster adjusting valves reach their target values before the other valves have time to respond to the changes in pre-pressure. The slower valves then essentially adjust to a fixed setting of the fast valves.

3.7.4 Air heaters

To control the air temperature at the air inlet of the absorber and regenerator, two 500 W electric air heaters are inserted into the air duct. The heating coil inside can be regulated using a 4-20 mA input signal. They have an inbuilt safety system, which prevents power from moving through the coil if the air flow rate is too low, as this could lead to overheating. This is accomplished by an inserted pipe, connected to a switch in the control chamber. This safety system also prevents the heating coil from turning on, if the heater is mounted the wrong way round, as no air would be forced down the tube. The air heater in the absorption cycle is only minimally used, due to the high heat losses. The air heater on the regeneration side however has a very important role in adjusting the incoming temperature at the regenerator. The feedback for the air heater is the temperature sensor of the air in front of the regenerator. Its control parameters are set to reach the target value as fast as possible, as the power throughput can be adjusted almost instantaneously. The fast controls of the air heater is also important for the control of the air cooler in the regeneration section. The parameters of the air cooler are set to respond much slower, so the temperature is almost stationary. As is it provides more cooling power at a constant air temperature, the humidity of the air starts to drop due to condensation. The system works very well, as long as the air heater manages to keep the temperature constant. Once the air heater looses the ability to regulate the temperature, the humidity increases with higher cooling power, as the effect of lowering the humidity through condensation is weaker than the effect of cooling the air. This leads to a false sign in the feedback, resulting in the mixing valve to settle in one of the extreme positions. This can happen either if the air heater reaches its maximum capacity, or if it turns itself off, which can happen in experiments with low air flow rate.

3.7.5 Water heaters

One of the main purposes of the test rig is to test the performance of the absorber and its ability to prevent frost formation on the air cooler. The most interesting region is the limit, where the air cooler just is or just isn't accumulating frost. To get rid of the ice on the air cooler between test runs, a heating rod is mounted right in front of the air cooler inlet. It is separated from the 230 V AC supply by a solid state relay. This allows to regulate the heating power by sufficiently fast pulse width modulation. The power output had to be limited, as else the heating rod might overheat. Especially at low flow rates the Leidenfrost-effect can cause problems, where the steam created through the heat insulates the heating rod. The rod is mounted inside the inlet pipe through a compression fitting. Radiators are positioned on the outside of the fitting, as without them it is possible for the fitting to overheat and get damaged. As an additional safety component a thermal switch which turns itself of at 60 °C is mounted on top of the outside tube and is connected in series with the power supply of the heating rod.

3.7.6 Fans

There are three fans used in the test rig. A controllable Rosenberg EC fan R200 in the absorption section and a controllable R125 in the regeneration section drive the air flow inside the test rig, while a non controllable AC R160 fan drives the fume hood on top. The fume hood was installed to remove potentially harmful aerosols of the desiccant. It has two large funnels, one above the absorber and the absorber tank, and one above the regenerator and the regenerator tank. They are connected through an air duct to the fan which then leads to the outside of the research facility. The fume hood fan can't be controlled and is always running at its maximum power. The two fans inside the test rig are controllable via a 0-10 V signal.

3.8 Limitations

The biggest obstacle for operating the test rig are the heat losses. On the regeneration cycle this is not as big of an issue as the absolute temperature difference to the surrounding area and the surface area are lower. On the absorption cycle however the introduction of heat causes a lot of problems, as the system of bath thermostats initially could not provide enough power to overcome them and reach target temperatures. In addition to the losses to the surrounding, the steam lance also introduces a lot of heat, and it cannot be fully replaced by the ultrasonic humidifier, as the humidity level can not be controlled without it. In order to achieve temperatures of interest at the absorber, the cycles have to be run in batch operation. Ideally the temperature of the absorber and the air cooler

could be adjusted separately, while the temperature at the absorber entrance is set using the heating register. However at a fixed temperature of the absorber, the air cooler has to use the remaining cooling power, to achieve useful conditions to test the absorber. This problem still prevails at lower air speeds. Also the gear pumps at the absorption cycle had problems working at high viscosity levels. This also only happens at the absorption cycle, where the disiccant concentration is high and its temperature are low. The air flow straightener build into each cycle create a lot of pressure drop, so testing carry over at high air velocities is not possible.

4 Results & discussion

Aim of this work was the transformation of two fin and tube heat exchangers into falling film absorbers using 3D printed parts and to make them affordable while providing a high performance. The designed inserts are able to sufficiently wet the fins of the falling film absorbers with desiccant, even at sub zero temperatures. Also, the falling film remains stable and without any desiccant losses caused by carry over into the air. There is certainly room for improvement, but the prototypes meet the requirements. Another main focus was to determine the performance of the absorber and the regenerator and the results look promising. For this a test rig was build, which is able to accurately control the conditioning of the air both in the absorption and regeneration cycle. The absorber and regenerator were tested separately, as the cooling power provided by the two bath thermostats was not sufficient to operate both simultaneously. The regenerator was tested first, because the water content of the desiccant was too high to test the absorber. The testing of the regenerator showed that the back flow of desiccant to the tank can be accomplished just by gravity, without the help of additional pumping. There were no problems with carry over of desiccant to the air, which was one of the larger concerns of this setup. The regenerator was tested at multiple desiccant flow rates, however there was no significant increase in water transfer, which suggests sufficient coverage of the fins by desiccant. After the desiccant was regenerated to a concentration of 80%, it was transferred over to the absorber tank. The testing of the absorber proved more difficult, due to the high viscosity at the low temperatures, occasionally causing failure in the shovel wheel pump at the back flow. The safety measures in the resistance measurement by the liquid sensor proved to be very useful, as it prevented the drip tray from spilling into the air duct multiple times, when the shovel wheel pump stopped. Similar to the regenerator, the fins seem to be sufficiently covered, and the system is working as expected. The desiccant used shows to be capable of efficiently transferring the water into and out of the air. It remains liquid at operation temperatures, without any detectable formation of crystals. The viscosity increases significantly at low temperatures, causing problems for shovel wheel pumps, while still being manageable by gear pumps.

4.1 Calibration

All of the temperature, humidity, Coriolis, vortex and magnetic flux sensors, as well as the hot wire anemometers where calibrated at AIT facilities, giving an estimate of their accuracy and the expected error. The biggest uncertainties for determination of the performance of the absorber and regenerator are introduced by the humidity sensors, as they tend to loose their accuracy over time at the high relative humidity. There are also some questions about the accuracy of the desiccant concentration calculated from the density measurement done by the Coriolis flow sensors and the temperature. All the data used to create the following plots is provided in the appendix. All calibrations use

linear spline functions. That way the errors of the individual measurements have a larger impact, however higher order terms are not disregarded entirely. To show the linearity of the measurements the linear fit is shown in each calibration graph.

4.1.1 Temperature Sensors

The PT100 are very accurate and only needed slight adjustments to be calibrated. They were all compared to a verifiable externally calibrated 4-wire resistance temperature detector, which was mounted in a shared water reservoir. All sensors were calibrated for a temperature range of -20 °C to 80 °C (shown in Fig. 26), as the lowest temperatures in our test rig won't fall below -11 °C while the highest won't exceed 60 °C. Each temperature was kept constant inside the bath for 5 minutes once it was stable and the bath temperature was set to 11 equally spaced temperature points. The linear spline function used to calibrate the temperature based on the measured resistance consists of ten segments that join the closest two calibration measurements. As all the measurements show very similar results, the temperature measurements can be considered very reliable.

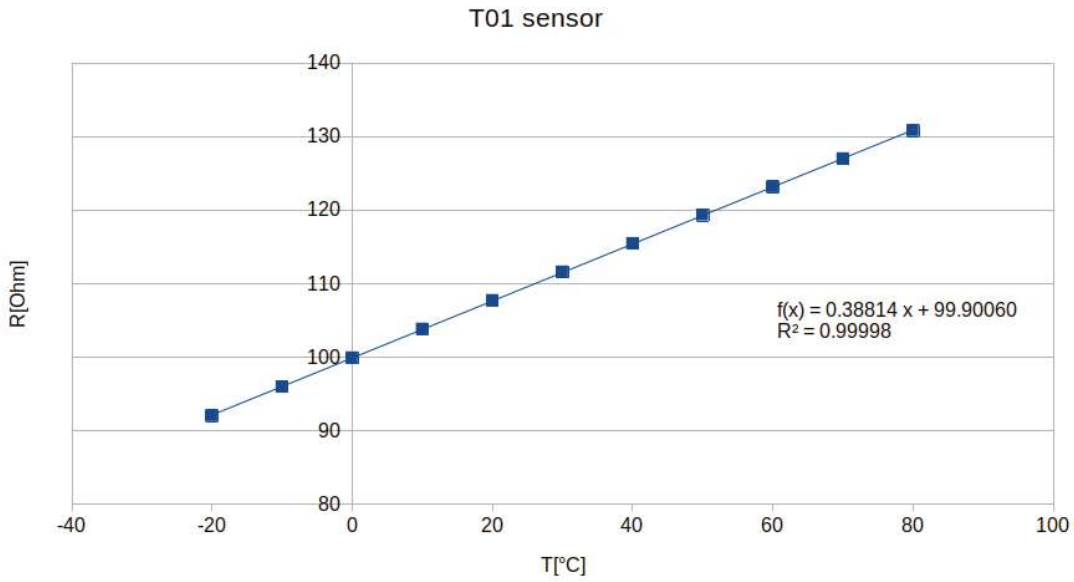

Figure 26: The resistance measured at 11 input temperatures of the T01 sensor and a linear fit showing how little the higher order terms contribute.

4.1.2 Humidity Sensors

The humidity sensors have their own internal PT100 sensor, which is needed to calculate the absolute water content of the air. Both the humidity sensor and the internal temperature sensor were calibrated separately. The internal PT100 sensors were calibrated inside the air ducts. This was done, because they are mounted only about two millimeters away from the extremely fragile capacitive humidity sensors, which made it impossible to calibrate them inside the water reservoir. They where compared to the already calibrated PT00 sensors inside the air duct. The temperature sensors where extremely reliable as seen in Fig. 27. The humidity sensors came calibrated by the manufacturer, however

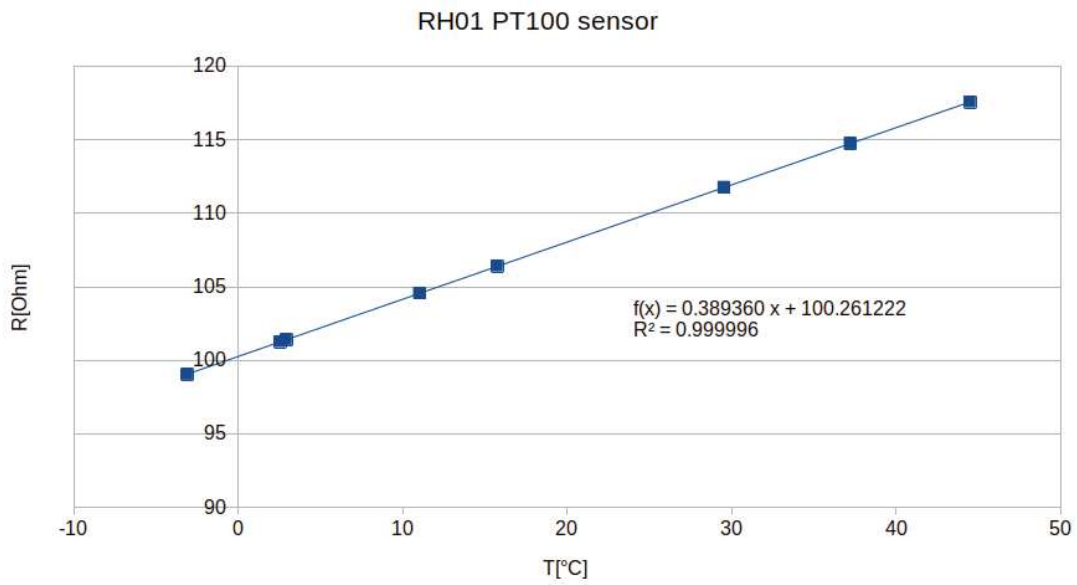

Figure 27: The resistance measurement of the internal temperature sensor of the humidity sensor RH01, taken at different temperatures set inside the air duct.

when they were compared to each other, they showed significant inaccuracies after some time in use. This can happen when the sensors remain at very high relative humidity for extended periods of time. After cleaning the sensors in an ultrasonic bath of isopropanol and then deionized water, they were mounted inside the air duct and calibrated using a verifiable externally calibrated EE33 reference sensor. In Fig. 28 the output voltages of all five sensors is shown at different humidity levels. The relative error is especially dominant at low humidity levels, while diminishing at higher ones. Similarly to the temperature sensors, a linear spline function was used rather than using the trend line. In order to be able to rely on the measurement data of the humidity sensors, they have to be re-calibrated regularly, especially after long exposure of air close to the dew point.

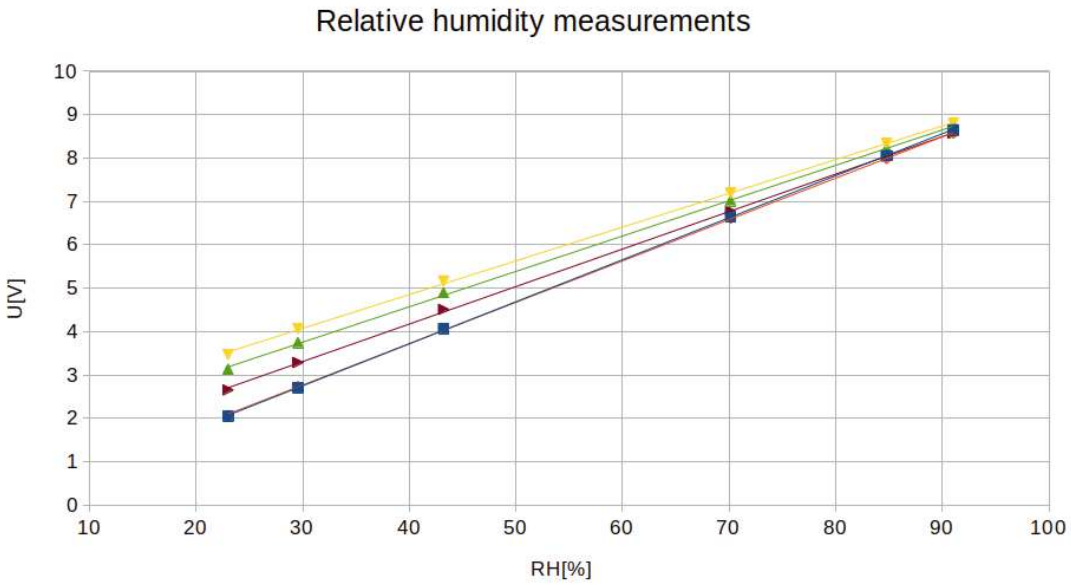

Figure 28: The calibration measurements of the humidity sensors showing a disagreement of over 10 % relative humidity at low voltage values.

4.1.3 Coriolis Sensors

The Coriolis sensors were calibrated by connecting them in series to a reference sensor, as seen in Fig. 29. Their output only deviated very slightly from their measurements. Because of their extremely high accuracy, they were used to calibrate the magnetic flux flow sensor and the vortex flow sensors.

4.1.4 Magnetic flux flow sensor

For the magnetic flux flow sensor the results were very comparable to the Coriolis flow sensors, which is important for an accurate energy balance over the regenerator, as there is no additional Coriolis, to confirm the water flow rate. The sensor was compared to a calibrated Coriolis sensor. The results are shown in Fig. 30.

4.1.5 Vortex Sensors

The vortex sensors were shown to be less reliable than the Coriolis and magnetic flux sensors. They were calibrated using a Coriolis sensor on the cooling cycle and the magnetic

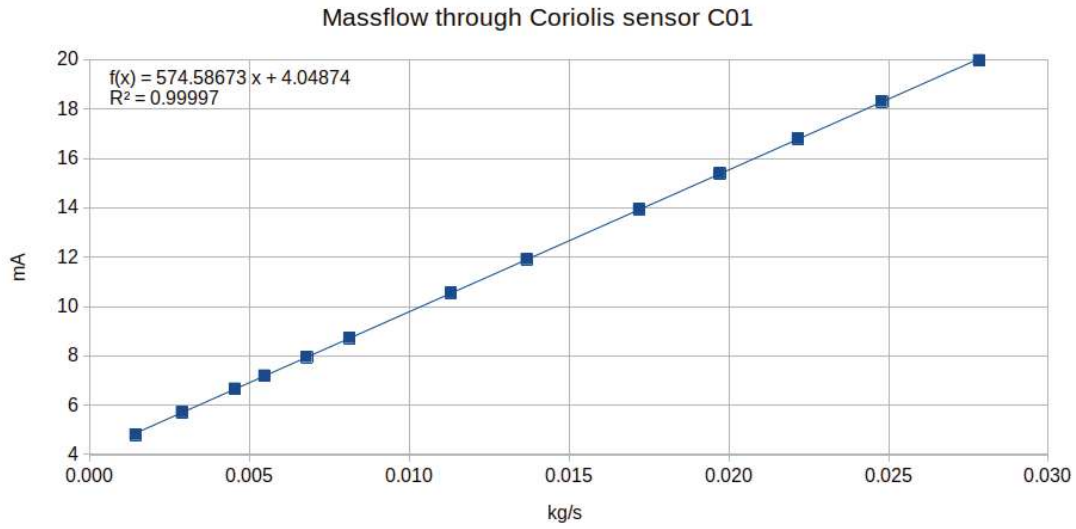

Figure 29: The output current of the Coriolis sensors on the y-axis are almost perfectly linear, when compared to the mass flow rate of the water on the x-axis.

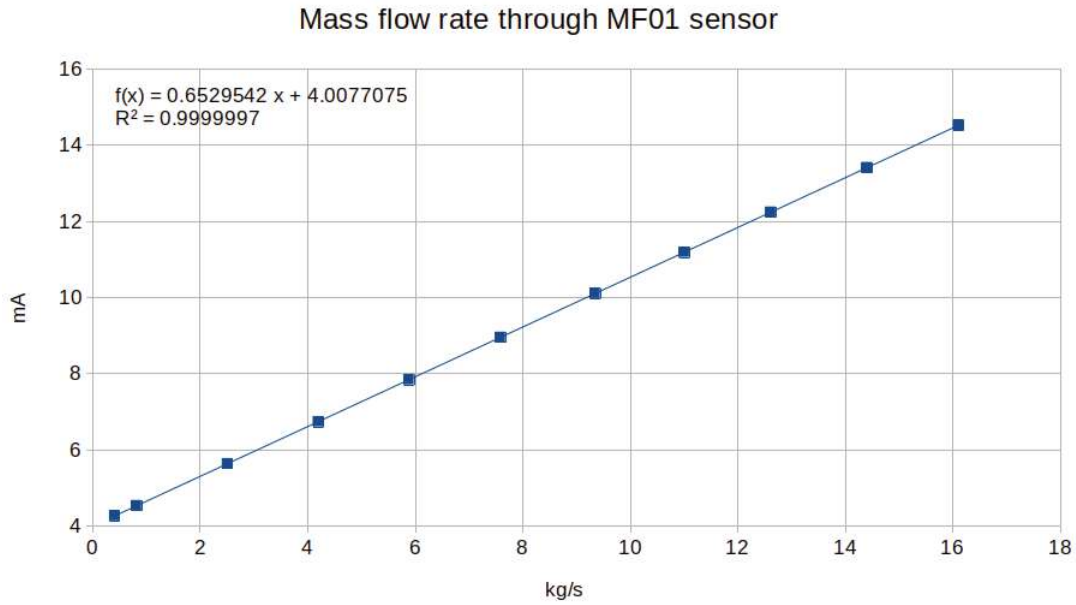

Figure 30: The output current of the magnetic flux flow sensor on the y-axis compared to the mass flow rate measured by the calibrated Coriolis using water on the x-axis.

flux sensor on the heating cycle. The measurements on the heating cycle using water show the expected results, however the high viscosity of the ethylene glycol seems to cause problems for the accuracy of the sensors in the cooling cycle. Their measurements are highly dependant on the viscosity, as seen in Fig. 31, Fig. 32 and Fig. 33. The output becomes non linear at certain flow rates at differing temperatures. In Fig. 31 the vortex flow meter of the absorber was tested at three different temperatures levels, spanning the typical operation temperature. At low flow rates the output shows a linear behaviour to the flow rate, however at higher flow rates the vortex street seems to have a more complicated behaviour than described in eq. 13. This results in a significant error, which happens earlier at lower temperatures where the viscosity increases. At the lowest measured temperature the linearity brakes at about 2.5 l/min. This represents the worst case scenario. For the calibration only the measurements up to the maximum flow rate of 2.5 l/min were used, which limits the range of operation for the pumps. In contrast to the other calibrations done so far, the accuracy of the individual measurements is not as high, so a linear regression was used as seen in Fig. 34(yellow).

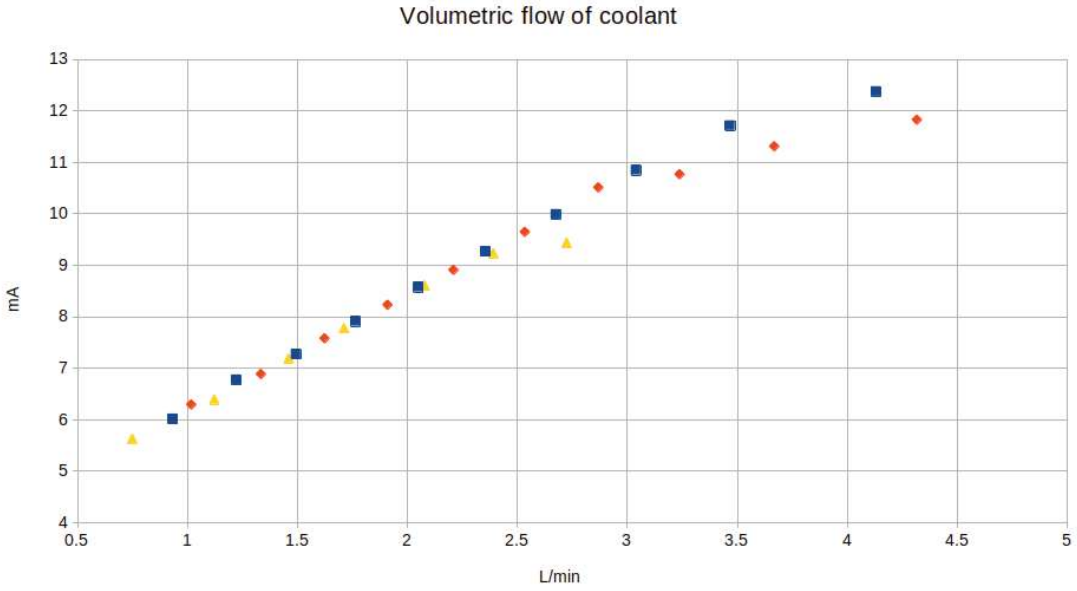

Figure 31: The absorber vortex sensor output current on the y-axis at temperatures between -4 °C (yellow), 1.5 °C (red) and 7.5 °C(blue), compared to the volumetric flow rate, calculated using the measurements by the Coriolis sensor, on the x-axis.

The vortex flow meter of the air cooler in the absorption cycle was calibrated at five different temperatures as seen in Fig. 32. Again there seems to be a break off point, where the vortex street starts to behave much less predictable, which changes with viscosity. For lower temperature this happens at lower flow rates and the maximum flow rate used for the calibration was set to 2.1 l/min. This is somewhat limiting, however at higher

temperatures (blue and orange) the linear fit is still a decent approximation even at higher flow rates. It should be said that the temperature at each of the same colored data points differs slightly. The reason for this is that the bath thermostat was set at a constant temperature, but as the vortex sensor is mounted at the heat exchanger exit. The temperature difference after the heat exchangers resulting from heat losses are a bit larger at lower flow rates, though this is a small effect. As seen in Fig. 34(orange), the data points of the calibration of the vortex sensor at the air cooler in the absorption cycle correlate well with the ones of the vortex sensor at the absorber, which is reassuring as they were taken at similar temperatures.

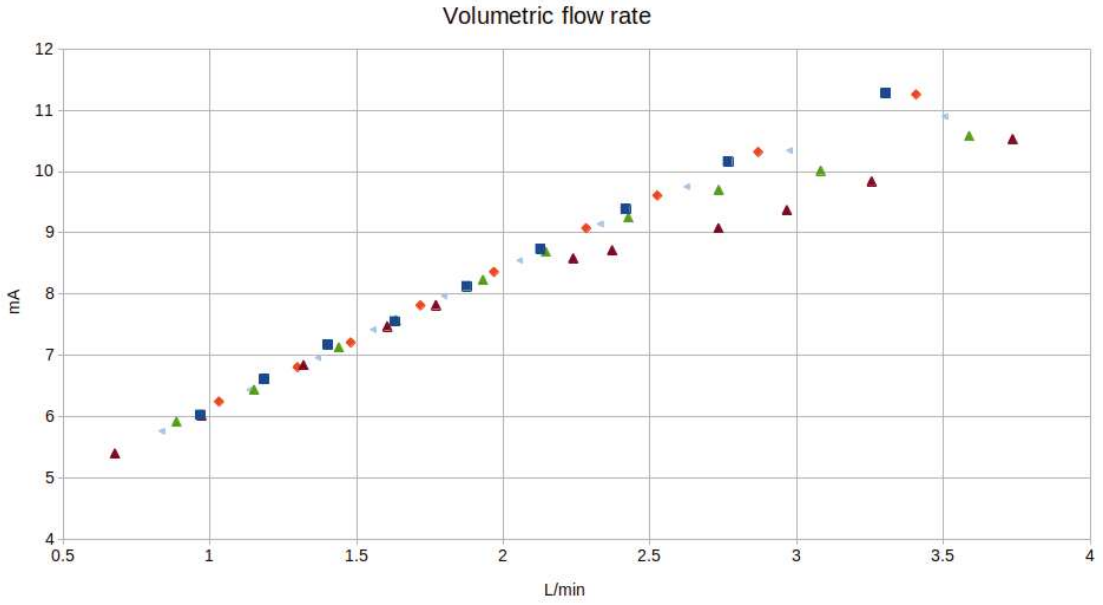

Figure 32: At the air cooler of the absorber section, it shows the linear behaviour of the vortex street with the discontinuity starting at 7.5 °C(blue), 2 °C(red), -0.6 °C(light blue), -4.5 °C(green) and -8 °C(purple).

The exit temperature range of the air cooler in the regeneration cycle is typically around 20 °C so the calibration was done at 15 and 25 °C. It also should be noted, that this calibration is not essential for the operation of the test rig, as the air cooler is only used to condition the air, and the control can be done without measuring the flow rate. However knowing the flow rates of all three parallel connections makes it possible to cross reference with the Coriolis measurement for validation. As seen in Fig. 33 the data points reach a discontinuity from the linear behaviour at some point between 1.5 and 2 l/min. The point at which this discontinuity starts, shifts at different temperatures similar to the calibration of vortex sensors in the absorption cycle. However, at some temperature it seems to becomes linear again. Interestingly in contrast to the low temperature data, this happens earlier at higher temperatures. It is possible that this discontinuity happens because the frequency of the vortex street reaches some interference point, but that

cannot explain the change in behavior at high temperatures. For the calibration the data points above 2 l/min were used, giving a minimum flow rate. The data points used for the linear approximation are shown in Fig. 34 (blue). In comparison to the low temperature measurements, there is a significant shift in the output, showing that the vortex sensors are strongly viscosity dependent.

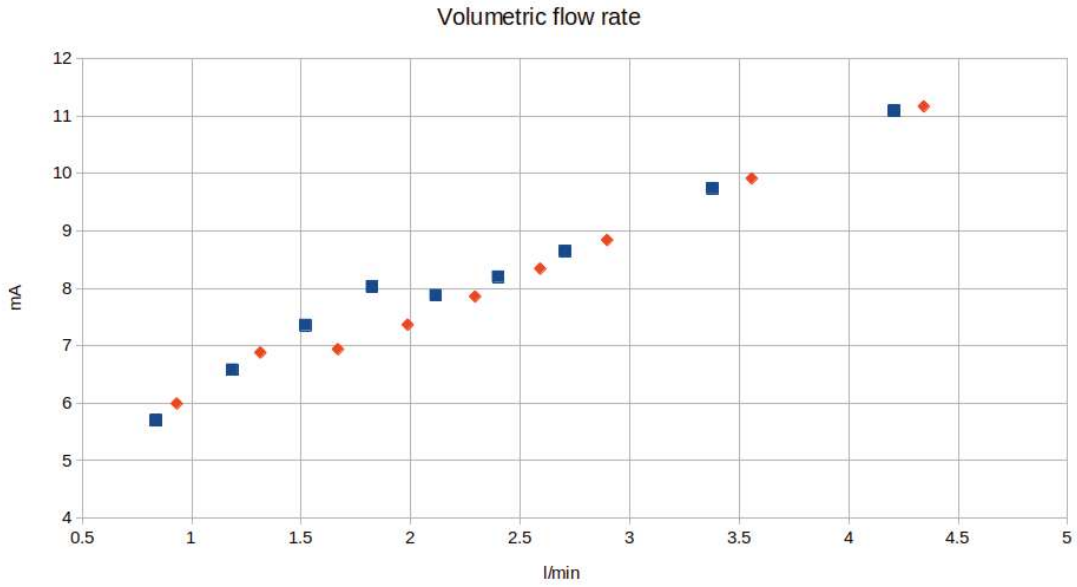

Figure 33: The calibration data of the vortex sensor at the air cooler in the regeneration section. The results at 15 °C are shown in blue and the results at 25 °C in red.

Overall the calibration of the vortex flow sensors comes with some limits in the range of validity, but their data fits well with the Coriolis measurement within its range of validity. Especially the low temperature data of the absorber section correlate very well with the linear approximation as seen in Fig. 34 (yellow and orange).

4.1.6 Hot wire anemometer

The calibration of the hot wire anemometer was done by calculating the mass flow of the air by energy balancing the heating/cooling power it provides. To calculate the mass flow, the air and the water/glycol solution temperatures both before and after the exchange as well as the mass flow of the coolant have to be measured. To mitigate the errors, the system was set up, so that the mass flow could be measured directly by a Coriolis sensor. Also, the temperature was set close to room temperature to minimize thermal losses to the environment. It is important to note, that this calibration only holds true for the precise position the anemometer is mounted in. Whenever it is moved, the calibration

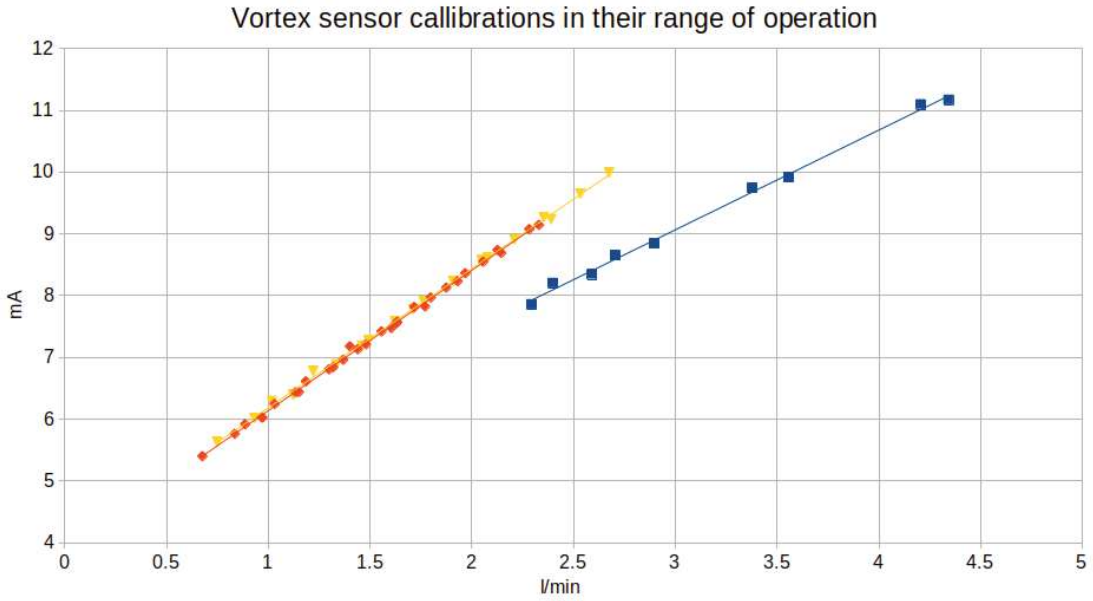

Figure 34: The low temperature calibration for the vortex sensor at the absorber (yellow) and the one at the air cooler (orange) on the absorber section correlate well, as they were done at similar temperature ranges. The data of the air cooler in the regeneration cycle (blue) deviates significantly.

has to be redone, as the position of the anemometer significantly alters its output because of the non uniformity of the air profile. This is not only true for vertical dispositions but also changes in rotation. The results are shown in Fig. 35. The value range for the regeneration cycle is smaller, because of the smaller fan. For low flow rates the sensors show similar results, while deviations are greater at higher air speeds. The calculated mass flow rates and the measured outputs individually do form a linear relationship. The data points have a higher deviation from the linear approximation than the previous calibrations. This was also expected, as the calculation depends on four temperature measurements and the mass flow measurement of the Coriolis, all contributing to the error. The high flow rate of over 430 kg/h on the absorption cycle during calibration could for some reason not be reproduced in later experiments.

4.2 Performance regenerator

The Fig. 36 shows the first test of the regenerator. The air(green) enters at a temperature of 30 °C with a relative humidity of 40 %, which represent very limiting conditions for real world applications and gets heated to 36.3 °C at 34.2 % relative humidity. As the hot water(blue) is cooled down by 2 °C, it provides about 430 W of heating power. A heating

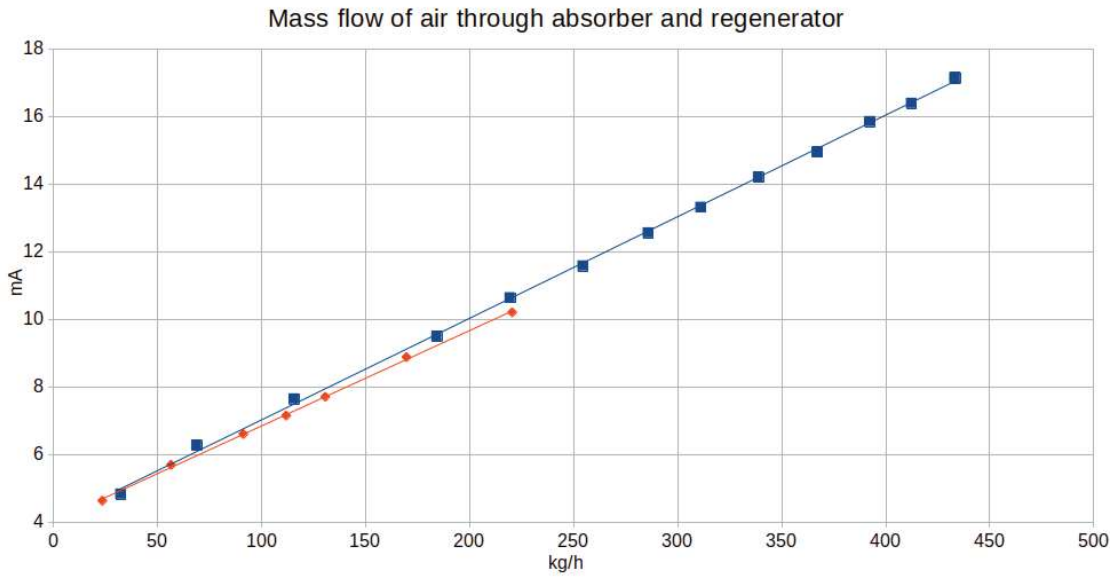

Figure 35: The output current of the hot wire anemometers on the y-axis are compared to the calculated mass flow rate of the air on the x-axis. The data of the absorber section is shown in blue and the data of the regenerator section in orange. The maximum air mass flow rate in the absorption section is almost twice as large as in the regeneration cycle, because of the larger fan and cross section. The maximum air velocity however is higher in the regenerator, due to its area being about one fourth that of the absorber.

power of 120 W is used to heat the desiccant. The difference of 310 W, separates to about 160 W sensible heating the air and 120 W, needed to evaporate the water into the air. The desiccant solution mass flow rate $\dot{m}_{\text{des}}$ of 3.6 g/min refers to the water flow rate from the desiccant to the air. This desorbed water content can be directly observed in the test rig at the air cooler in the regeneration cycle, where condensed water exits the ccollection tray through a clear hose. For these regeneration parameters, the concentration of the desiccant water solution was calculated to be at 79 %. The partial water vapor pressures is the driving force of the desorption. In the air it was calculated to be 1708 Pa at the inlet and 2074 Pa at the outlet. The partial water pressure of the desiccant is an estimate, created by averaging the partial pressures at the inlet and the exit. Calculating the real value proves difficult, as the desiccant concentration and temperature changes, while flowing down the fins.

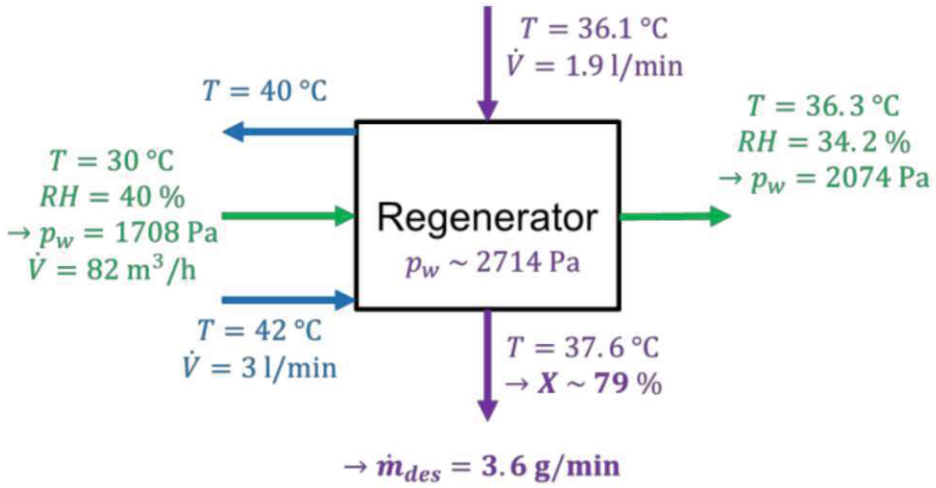

Figure 36: First test data of the regenerator, with the air properties shown in green, desiccant in purple and water in blue.

4.3 Performance absorber

The first test of the absorber is shown in Fig. 37. The ethylene glycol mixture provides about 930 W of cooling power to the absorber. 275 W of this are used to cool the desiccant by 3 °C. Of the remaining 655 W, 405 W are used for sensible cooling of the air, while 250 W are used to compensate for the energy freed by the phase change of the water vapor when absorbed into the desiccant. The air enters the absorber at 7 °C and 80 % relative humidity, representing standard conditions in a cold store, which results in a partial pressure of water vapor at 806 Pa. By removing the water, the partial pressure could be reduced to 496 Pa, which at the exit temperature of 0.2 °C, reduces the dew point to -2.55 °C. The ethylene glycol water solution entered the absorber at -7 °C, while the desiccant exits at only -0.6 °C. The mass flow of the water into the solution of 6.4 g/min looks promising. It is higher than in the regenerator, even though the difference in partial pressure is estimated to be more than twice as high at the regenerator. The reason for this is that the area of interaction is about four times higher on the absorber and the mass flow of the air is almost twice as high.

4.4 Possible improvements for the test rig

The biggest limitations for the system currently are the heat losses to the environment, because the bath thermostats are not able to provide enough cooling power to run both sides simultaneously. The test runs so far have the absorber or the regenerator operating separately, while exchanging only with their own desiccant tanks. Once the concentration

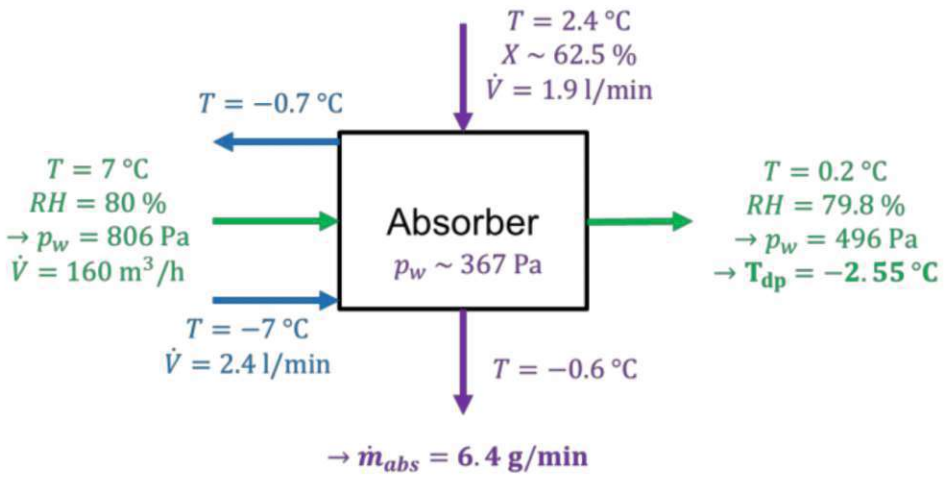

Figure 37: The first results for the absorber. The properties of the air are highlighted in green, desiccant in purple and water glycol solution in blue.

in the tank reaches a limiting concentration, the desiccant water solution is transferred to the other tank, where the experiments continue. In the future the situation might be improved, by separating the two bath thermostats between the absorption section and a regeneration section. This makes it possible for the thermostat of the air cooler on the hot side to run at higher temperatures making it more efficient. Alternatively, the insulation can be improved by adding another layer on top of the current one. This might also help to further decrease the air leakage, which is still present, even after applying silicone on all the air duct connections. This would also reduce the temperature increase along the duct of the absorption cycle, making it possible to reduce the temperature at the absorber, without having to increase the power of the air cooler. Once the losses are low enough, the air cooler could be set to a point of interest, while the conditioning of the inlet temperature of the absorber could be controlled by the heating register, as originally intended. Another limiting factor is the accuracy of the concentration measurement of the desiccant solution. Currently this is done by referencing the density data at set temperatures and mixing ratios, provided by the manufacturer, to the density measurement of the Coriolis. This proved to be problematic, as the calculations for the desiccant concentration at the two outlets of the same tank disagree by up to 5 %. This could not be reduced by mixing the tank, so the problem lies either in the density measurement of the Coriolis being inaccurate, or the data provided by the manufacturer being wrong. The density measurement of the Coriolis flow meters has not been calibrated at the AIT facilities yet. This poses a challenge, as a wide range of different liquid densities need to be tested for the full range necessary for the test rig. Also a problem for the test rig is the absorption of water directly into the desiccant tank, as the tank is directly connected to the air duct to prevent pressure from building up. Getting rid of this water takes the regenerator a lot of time, limiting the duration of the actual test

time in the desiccant concentration of interest. Right now this effect is amplified, because the system is only operated one side at a time, while the desiccant in the unused tank, accumulates water. This effect might be reduced, by adding a valve into the connector, which opens at very low pressure, but stops any additional air exchange.

5 Conclusion & future research

The test rig provides most of the desired features to experiment with varying air conditions, opening a lot of options for future research. The desiccant can easily be replaced, to test the performance of different absorption liquids. There are numerous safety features built in, which already proved their usefulness. Even with the current limitations, the test rig proved to be able to give accurate test results of the efficiency of the absorber and regenerator, which was the main goal of this project. The construction of the falling film absorber and regenerator was a great success, showing that it is possible to reliably create a stable falling film on an fin and tube heat exchanger using cheap materials that are easy to produce.

Looking forward there are still possible improvements to the test rig like the addition of extra insulation material to the absorption cycle to reduce thermal losses. Also the direct air exchange of the desiccant tanks with the air ducts should be limited, to reduce the efforts of conditioning the desiccant. The density measurement of the Coriolis sensors should be calibrated to increase the accuracy of the desiccant concentration data.

The use of ionic liquid as desiccant proved to be managable to work with, even at the high viscosity at low temperatures. Carry over of the desiccant into the air proved to not cause any significant losses, as after a full test run of both sides no desiccant droplets could be detected exiting the back end of the falling film and the filters showed no signs of desiccant deposition. The absorber being able to reduce the dew point to -2.5 °C shows that this method can be used to dehumidify the air in cold stores, even at these low temperatures and low absolute humidities. The desiccant concentration needed to accomplish this can easily be reached by the regenerator at only 40 °C, where the partial pressure of water in the air was still increasing from 1708 Pa to 2074 Pa.

The results of the first tests show the viability of the system, however further research is needed to fully test the performance of the system and its limitations. There are several things to test and optimize like the choice of desiccant, air speed, temperature, humidity, desiccant concentration, desiccant exchange rate, both between the tanks and into the falling films, and the coolant temperature and flow rate. During the testing also the question emerged, if it might be beneficial to eliminate the use of the air cooler, by shifting all of the sensitive cooling load to the absorber. It would be a lot easier to upgrade the air coolers in cold stores to falling film absorbers, rather than installing a separate device.

List of Figures

List of Tables

References

[1] Abd-Elhady, M. M., Salem, M. S., Hamed, A. M., and El-Sharkawy, I. I. (2022). Solid desiccant-based dehumidification systems: A critical review on configurations, techniques, and current trends. *International Journal of Refrigeration*, 133:337–352.

[2] Ali, A., Vafai, K., and Khaled, A.-R. (2004). Analysis of heat and mass transfer between air and falling film in a cross flow configuration. *International Journal of Heat and Mass Transfer*, 47(4):743–755.

[3] Arroiabe, P., Martinez-Agirre, M., and Bou-Ali, M. M. (2022). Numerical analysis of different mass transfer models for falling film absorbers. *International Journal of Heat and Mass Transfer*, 182:121892.

[4] Bruus, H. (2007). *Theoretical microfluidics*, volume 18. Oxford university press.

[5] Elsayed, S., Miyazaki, T., Hamamoto, Y., Akisawa, A., and Kashiwagi, T. (2008). Performance analysis of air cycle refrigerator integrated desiccant system for cooling and dehumidifying warehouse. *International journal of refrigeration*, 31(2):189–196.

[6] Emhofer, J., Beladi, B., Dudzinski, P., Fleckl, T., and Kuhlmann, H. C. (2017). Analysis of a cross-flow liquid-desiccant falling-film. *Applied Thermal Engineering*, 124:91–102.

[Heinze et al.] Heinze, R., Biedermann, T., Kameier, F., and Paschereit, O. Modellbildung der schalldruckverstärkung an einer zylinder-platte-konfiguration.

[8] Hochwallner, F., Stephani, B. L. L., Emhofer, J., Fleckl, T., and Reichl, C. (2023). Experimentelle untersuchung eines frost-präventionssystems für kühlhäuser. In *DKV-Tagung 2023*.

[9] Karel, M. and Lund, D. (2003). *Physical principles of food preservation: revised and expanded*. CRC Press.

[10] Kim, W. R., Aung, M. M., Chang, Y. S., and Makatsoris, C. (2015). Freshness gauge based cold storage management: A method for adjusting temperature and humidity levels for food quality. *Food control*, 47:510–519.

[11] Lazzarin, R., Gasparella, A., and Longo, G. A. (1999). Chemical dehumidification by liquid desiccants: theory and experiment. *International Journal of Refrigeration*, 22(4):334–347.

[12] Liu, H., Yang, H., and Qi, R. (2020). A review of electrically driven dehumidification technology for air-conditioning systems. *Applied Energy*, 279:115863.

[13] Mahamoudou, A., Le Pierrès, N., and Ramousse, J. (2022). Review of coupled heat and mass transfer studies in falling film absorbers: Modeling, experimental and thermodynamic approaches. *International Journal of Refrigeration*, 136:229–244.

[14] Pineda, S. M. and Diaz, G. (2011). Performance of an adiabatic cross-flow liquid-desiccant absorber inside a refrigerated warehouse. *international journal of refrigeration*, 34(1):138–147.

[15] Stephan, K. (1959). Wärmeübergang und druckabfall bei nicht ausgebildeter laminarströmung in rohren und in ebenen spalten. *Chemie Ingenieur Technik*, 31(12):773–778.

[16] Su, W., Lu, Z., She, X., Zhou, J., Wang, F., Sun, B., and Zhang, X. (2022). Liquid desiccant regeneration for advanced air conditioning: A comprehensive review on desiccant materials, regenerators, systems and improvement technologies. *Applied Energy*, 308:118394.

Appendix

A Measurement data

C01		C02		C05		C03		C07		C08		C06	
Ref(kg/s)	Out(mA)	Ref(kg/s)	Out(mA)	Ref(kg/s)	Out(mA)	Ref(kg/s)	Out(mA)	Ref(kg/s)	Out(mA)	Ref(kg/s)	Out(mA)	Ref(kg/s)	Out(mA)
0.00143	4.80006	0.00143	4.74608	0.24731	18.24486	0.22527	16.92121	0.00174	4.94351	0.00174	4.93008	0.01191	4.67787
0.00288	5.71287	0.00288	5.58234	0.22295	16.84181	0.19516	15.19327	0.00365	6.04780	0.00365	6.03894	0.01236	4.70303
0.00454	6.66802	0.00454	6.53394	0.19460	15.20864	0.16720	13.58822	0.00515	6.91916	0.00515	6.90360	0.05067	6.90911
0.00546	7.19748	0.00546	7.06757	0.16697	13.61746	0.13938	11.99170	0.00688	7.91101	0.00688	7.90010	0.09994	9.74594
0.00678	7.95449	0.00678	7.82620	0.13895	12.00292	0.11145	10.38889	0.00922	9.25929	0.00922	9.24467	0.14924	12.58471
0.00812	8.72479	0.00812	8.59632	0.11114	10.40135	0.08364	8.79248	0.01092	10.24036	0.01092	10.22402	0.18526	14.66015
0.01130	10.55122	0.01130	10.42551	0.08333	8.79919	0.05576	7.19260	0.01440	12.25177	0.01440	12.23799		
0.01367	11.91624	0.01367	11.79218	0.05556	7.19976	0.02777	5.58525	0.01635	13.37757	0.01635	13.36875		
0.01719	13.94106	0.01719	13.82200	0.02774	5.59758	0.01388	4.78766						
0.01972	15.39339	0.01972	15.27815	0.01351	4.77748	0.00707	4.39679						
0.02216	16.79925	0.02216	16.68471	0.00832	4.47870								
0.02479	18.31168	0.02479	18.19827	0.00407	4.23405								
0.02784	19.97893	0.02784	19.95530										

Table 1: The calibration measurements for the Coriolis sensors.

Reference (kg/s)	Measurement (mA)
2.5049	5.6431
0.8142	4.5417
0.4077	4.2759
4.1956	6.7427
5.8809	7.8456
7.5806	8.9569
9.3441	10.1111
11.0038	11.1922
12.6101	12.2424
14.4017	13.4119
16.1004	14.5206

Table 2: The calibration measurements for the magnetic flow sensor.

	T01		T02		T03		T04		T05		T06	
Set point	T[°C]	R[Ohm]	T[°C]	R[Ohm]	T[°C]	R[Ohm]	T[°C]	R[Ohm]	T[°C]	R[Ohm]	T[°C]	R[Ohm]
-20	-20.02	92.03	-20.02	92.03	-20.02	92.07	-20.01	92.08	-20.02	92.05	-20.02	92.01
-10	-10	95.98	-10	95.98	-10	96.01	-10	96.03	-10	96	-10.01	95.95
0	0	99.91	0	99.91	0	99.94	0	99.95	-0.01	99.93	0	99.88
10	10	103.82	10	103.82	10	103.86	10	103.87	10	103.85	10	103.8
20	20	107.72	20	107.72	20	107.76	20	107.77	20	107.75	20	107.7
30	30	111.61	30	111.61	30	111.65	30	111.66	30	111.64	30	111.58
40	40.01	115.49	40	115.49	40.01	115.52	40	115.53	40	115.52	40.04	115.47
50	50	119.35	50	119.35	50.04	119.4	50	119.4	50	119.38	50	119.32
60	60	123.2	60	123.2	60	123.23	60.04	123.26	60.01	123.23	60	123.17
70	70	127.03	70	127.04	70.04	127.08	70	127.08	70.03	127.07	70.04	127.02
80	80	130.85	80	130.86	80	130.89	80.04	130.91	80.01	130.89	80.01	130.83
	T07		T08		T09		T10		T11		T12	
Set point	T[°C]	R[Ohm]	T[°C]	R[Ohm]	T[°C]	R[Ohm]	T[°C]	R[Ohm]	T[°C]	R[Ohm]	T[°C]	R[Ohm]
-20	-20.02	92.02	-20.01	92.04	-20.02	92.05	-20.02	92.05	-20.02	92.03	-20.02	92.03
-10	-10.01	95.96	-10	95.99	-10	96	-10	95.99	-10.01	95.98	-10.01	95.98
0	0	99.89	0	99.91	0	99.93	0	99.92	-0.01	99.91	-0.01	99.91
10	10	103.81	10	103.83	10	103.84	10	103.84	10	103.82	9.99	103.83
20	20	107.71	20	107.73	20	107.74	20	107.74	20	107.73	20	107.73
30	30	111.6	30	111.62	30	111.63	30	111.63	30	111.62	30	111.62
40	40.04	115.49	40	115.49	40.01	115.51	40.01	115.5	40	115.49	40	115.49
50	50	119.33	50	119.35	50	119.37	50	119.36	50	119.35	50	119.36
60	60	123.18	60.01	123.2	60	123.22	60	123.21	60	123.2	60.03	123.22
70	70.01	127.02	70	127.03	70.01	127.06	70.01	127.04	70	127.04	70.01	127.04
80	80.01	130.84	80	130.85	80.03	130.89	80.04	130.88	80.01	130.86	80.01	130.87
	T13		T14		T15		T16		T17		T18	
Set point	T[°C]	R[Ohm]	T[°C]	R[Ohm]	T[°C]	R[Ohm]	T[°C]	R[Ohm]	T[°C]	R[Ohm]	T[°C]	R[Ohm]
-20	-20.02	92.03	-20.02	92.05	-20.01	92.02	-20.01	92.03	-20.02	92.03	-20.02	92.05
-10	-10.01	95.98	-10.01	96	-10	95.97	-10	95.98	-10.01	95.98	-10.01	96
0	-0.01	99.91	0	99.93	0	99.9	0	99.91	0	99.9	0	99.93
10	10	103.82	10	103.84	10	103.82	10	103.82	9.99	103.82	10	103.85
20	20	107.73	20	107.75	20	107.72	20	107.73	20	107.72	20	107.75
30	30	111.62	30	111.64	30	111.6	30	111.62	30	111.61	30	111.64
40	40	115.49	39.99	115.51	40.01	115.48	39.99	115.49	40	115.49	40	115.51
50	50	119.35	50	119.38	50	119.34	50	119.35	50.04	119.36	50	119.38
60	60	123.2	60.01	123.23	60	123.19	60.01	123.2	60	123.19	60	123.23
70	70.04	127.05	70	127.06	70	127.03	70	127.04	70	127.03	70.01	127.06
80	80.01	130.86	80	130.89	80	130.85	80	130.86	80	130.85	80.04	130.9
	T19		T20		T21		T22		T23		T24	
Set point	T[°C]	R[Ohm]	T[°C]	R[Ohm]	T[°C]	R[Ohm]	T[°C]	R[Ohm]	T[°C]	R[Ohm]	T[°C]	R[Ohm]
-20	-20.02	92.05	-20.02	159.53	-20.01	152.81	-20.01	92.05	-20.01	92.07	-20.02	92.04
-10	-10	96	-10.01	155.04	-10.01	131.21	-10.01	96	-10	96.01	-10.01	95.98
0	0	99.93	0	158.91	-0.01	160.63	0	99.93	0	99.94	-0.01	99.91
10	10	103.85	10	162.45	10	138.53	10	103.85	10	103.86	10	103.83
20	20	107.75	20	141.26	20	167.74	20	107.75	20	107.76	19.98	107.73
30	30	111.64	30	177.51	30	171.15	30	111.64	30	111.65	30	111.62
40	40.03	115.53	40	181.06	40	149.63	40	115.51	40	115.53	40	115.5
50	50	119.38	50	152.26	50	153.32	50	119.38	50	119.39	50	119.36
60	60.03	123.24	60	155.98	60	157.08	60	123.23	60	123.24	60	123.21
70	70	127.07	70	183.25	70	160.82	70.04	127.08	70	127.08	70	127.04
80	80.04	130.9	80.04	187.26	80	196.86	80	130.89	80	130.9	80	130.87
	T25		T26		T27		T28		T29		T30	
Set point	T[°C]	R[Ohm]	T[°C]	R[Ohm]	T[°C]	R[Ohm]	T[°C]	R[Ohm]	T[°C]	R[Ohm]	T[°C]	R[Ohm]
-20	-20.02	92.03	-20.01	92.02	-20.02	92.03	-20.02	92.03	-20.01	92.04	-20.01	92.04
-10	-10.01	95.98	-10.01	95.96	-10.01	95.98	-10.01	95.98	-10	95.99	-10	95.98
0	-0.01	99.91	0	99.89	0	99.91	-0.01	99.91	0	99.91	0	99.91
10	9.99	103.82	10	103.8	10	103.82	10	103.83	10	103.83	10	103.83
20	20	107.72	20	107.7	19.99	107.73	20	107.73	20	107.73	20	107.73
30	30	111.61	30	111.59	30	111.62	30	111.62	30	111.62	30	111.62
40	40	115.49	40	115.47	40	115.49	40.03	115.51	40	115.5	40	115.5
50	50.04	119.37	50	119.33	50	119.36	50	119.36	50	119.36	50	119.36
60	60	123.2	60	123.18	60	123.2	60	123.21	60	123.21	60	123.21
70	70	127.04	70.04	127.02	70	127.04	70	127.04	70	127.04	70	127.04
80	80	130.86	80.01	130.83	80	130.86	80	130.87	80	130.87	80	130.87
	T31		T32		T33		T34		T35		T36	
Set point	T[°C]	R[Ohm]	T[°C]	R[Ohm]	T[°C]	R[Ohm]	T[°C]	R[Ohm]	T[°C]	R[Ohm]	T[°C]	R[Ohm]
-20	-20.02	92.03	-20.01	92.07	-20.01	92.06	-20.02	92.03	-20.01	92.03	-20.01	92.04
-10	-10.01	95.98	-10.01	96.02	-10	96.01	-10.01	95.98	-10	95.97	-10	95.99
0	-0.01	99.91	0	99.95	0	99.93	-0.01	99.91	0	99.9	-0.01	99.92
10	10	103.82	10	103.87	9.99	103.85	10	103.82	10	103.82	10	103.83
20	20	107.73	20	107.77	20	107.75	20	107.73	20	107.72	20	107.73
30	30	111.61	30	111.66	30	111.64	30	111.62	30	111.61	30	111.62
40	40	115.49	40	115.54	40	115.52	40	115.49	40	115.48	40	115.5
50	50	119.35	50	119.4	50	119.38	50.04	119.37	50	119.34	50	119.36
60	60	123.2	60	123.25	60	123.23	60.03	123.21	60	123.19	60	123.21
70	70	127.04	70	127.09	70	127.07	70	127.04	70.04	127.04	70.03	127.06
80	80	130.86	80	130.91	80.04	130.9	80	130.86	80	130.85	80	130.87

Table 3: The calibration measurements for the temperature sensors.

1010F (%)	RH01 (V)	RH02 (V)	RH03 (V)	RH04 (V)	RH05 (V)
23.00757	2.65260	3.12808	3.46560	2.06242	2.04896
29.56901	3.28492	3.74272	4.06756	2.72658	2.70194
43.22274	4.50881	4.89216	5.16283	4.07293	4.06639
70.15096	6.77586	7.01528	7.19130	6.60947	6.65178
84.77162	8.04065	8.21872	8.33609	7.98777	8.05132
91.03968	8.57109	8.72951	8.80474	8.57357	8.64906

Table 4: The calibration measurements for the humidity sensors.

T[°C]	rho[kg/m³]	$\dot{m}$[kg/h]	I[mA]	$\dot{V}$[l/min]
-4.01677	1040.53713	257.84414	12.37458	4.12998
-3.97124	1040.59030	216.47216	11.71115	3.46714
-3.90124	1040.70378	189.75242	10.84499	3.03885
-3.80338	1040.82985	167.03183	9.98848	2.67466
-3.64652	1040.56434	146.95623	9.26799	2.35379
-3.48604	1040.52953	127.92159	8.57415	2.04898
-3.25696	1040.74119	110.10559	7.90918	1.76326
-3.05668	1040.80203	93.27172	7.27206	1.49359
-2.72539	1040.36620	76.25304	6.77671	1.22157
-1.94808	1040.09332	58.22053	6.01739	0.93294
0.55479	1041.17532	269.58896	11.82454	4.31546
0.62945	1040.94681	229.05760	11.30941	3.66746
0.70127	1040.83708	202.14521	10.76609	3.23690
0.79226	1040.77240	179.07864	10.51021	2.86772
0.84873	1041.02067	158.24695	9.64755	2.53352
0.95723	1041.03190	137.99304	8.90866	2.20923
1.13714	1040.85502	119.25073	8.22986	1.90950
1.33901	1040.69573	101.35811	7.57881	1.62324
1.56661	1040.82134	83.29951	6.88537	1.33387
1.95406	1040.78689	63.54617	6.29386	1.01760
6.44984	1041.16629	170.16580	9.43626	2.72396
6.55299	1040.91772	149.28821	9.23565	2.39033
6.62166	1040.86680	129.77929	8.61170	2.07806
6.75067	1040.93349	106.92594	7.78188	1.71202
6.90362	1040.92414	91.22297	7.18877	1.46061
7.13298	1040.72965	70.08762	6.39252	1.12241
7.57673	1040.59136	46.80124	5.63020	0.74959

Table 5: Calibration measurements for the vortex flow sensor at the absorber.

T[°C]	rho[kg/m³]	$\dot{m}$[kg/h]	I[mA]	$\dot{V}$[l/min]
-8.04153	1040.80451	206.30591	11.28150	3.30363
-7.95820	1040.77840	172.72440	10.15985	2.76595
-7.82550	1040.81215	150.95325	9.38835	2.41723
-7.67328	1040.98206	132.82894	8.73672	2.12666
-7.48807	1040.83503	117.10132	8.12928	1.87512
-7.24557	1040.55604	101.75213	7.55325	1.62977
-6.97100	1040.43446	87.50495	7.17740	1.40174
-6.69859	1040.31165	73.97970	6.61137	1.18522
-6.41173	1040.31595	60.43282	6.03017	0.96818
-5.13815	1041.23879	212.84680	11.25755	3.40695
-5.02893	1041.03460	179.20642	10.31839	2.86904
-4.92768	1040.95841	157.70556	9.60776	2.52501
-4.83660	1041.01798	142.58180	9.07474	2.28273
-4.68736	1041.17707	122.96693	8.36154	1.96840
-4.50270	1040.98657	107.30399	7.81482	1.71799
-4.27519	1040.85739	92.44688	7.21028	1.48030
-4.04349	1040.80383	81.12503	6.80684	1.29908
-3.65259	1040.56668	64.39668	6.24561	1.03144
-2.22938	1041.55241	218.96596	10.89715	3.50384
-2.15812	1041.33063	185.89538	10.34171	2.97529
-2.06694	1041.24976	164.03433	9.75176	2.62560
-1.97351	1041.21922	145.57201	9.14344	2.33015
-1.88846	1041.44568	128.47613	8.54758	2.05605
-1.73869	1041.25881	112.37731	7.96860	1.79874
-1.56532	1041.08341	97.26164	7.41965	1.55706
-1.36902	1041.14873	85.50655	6.96142	1.36879
-1.05875	1040.97537	70.93066	6.43665	1.13564
-0.61530	1041.02010	52.22453	5.76290	0.83611
0.75171	1040.96548	224.10295	10.57970	3.58806
0.79554	1041.09912	192.52746	10.01551	3.08212
0.85577	1040.96763	170.80221	9.70118	2.73467
0.92589	1040.99761	151.56884	9.24899	2.42666
1.00329	1040.99727	133.98168	8.69129	2.14509
1.08376	1041.02326	120.61211	8.23268	1.93099
1.24069	1041.08886	102.07034	7.57501	1.63403
1.38342	1040.99942	89.93114	7.13042	1.43982
1.71187	1040.80801	71.87740	6.43950	1.15099
2.09884	1040.65935	55.36536	5.91674	0.88670

6.38625	1041.65630	233.50500	10.53179	3.73612
6.49310	1040.86034	203.31922	9.84009	3.25563
6.51512	1040.93907	185.28988	9.37287	2.96671
6.54303	1040.95932	170.74016	9.07608	2.73370
6.60662	1040.91220	148.10069	8.71651	2.37133
6.62596	1040.87651	139.81354	8.58485	2.23871
6.76857	1040.82882	110.58856	7.82242	1.77084
6.79611	1040.84123	100.23347	7.47476	1.60501
6.90292	1041.19563	82.43749	6.84099	1.31960
7.13908	1041.55043	60.71606	6.02565	0.97157
7.51505	1042.05942	42.31128	5.39928	0.67673

Table 6: Calibration measurements for the vortex flow sensor at the air cooler of the absorbtion cycle.

T[°C]	rho[kg/m³]	$\dot{m}$[kg/h]	I[mA]	$\dot{V}$[l/min]
15.21976	1040.43283	262.65101	11.09374	4.20740
15.23714	1040.34086	210.84914	9.74258	3.37789
15.25817	1040.35422	168.85678	8.65049	2.70512
15.27735	1040.42183	149.77240	8.20295	2.39923
15.29655	1040.38998	131.98370	7.88071	2.11433
15.31295	1040.64501	113.84483	8.02716	1.82331
15.35303	1040.73363	94.85466	7.36053	1.51904
15.42499	1040.65311	73.99184	6.58173	1.18502
15.54138	1040.91141	52.23565	5.70245	0.83638
25.00211	1038.72101	270.67483	11.16795	4.34308
25.01622	1039.06967	221.77878	9.91363	3.55733
25.00459	1039.03322	180.60560	8.84124	2.89701
24.99500	1039.12590	161.56105	8.34322	2.59130
24.98145	1039.29300	143.04152	7.85760	2.29389
24.95876	1039.54140	123.88618	7.36689	1.98623
24.95997	1039.24421	103.97817	6.93967	1.66753
24.93920	1039.08028	81.89467	6.88182	1.31358
24.90648	1039.16054	58.10328	5.99372	0.93189

Table 7: Calibration measurements for the vortex flow sensor at the air cooler of the regeneration cycle.

$T_{a(in)}$[°C]	$T_{a(out)}$[°C]	$T_{w(in)}$[°C]	$T_{w(out)}$[°C]	$\dot{m}_w$[kg/h]	$\rho_w[kg/m]$	I[mA]	$\dot{m}_a$[kg/h]	$\dot{m}_a$[kg/s]
25.61748	21.46291	13.84854	20.78216	69.46423	1039.84036	17.11913	433.29726	0.12036
25.81003	21.45773	13.86564	20.77717	69.47731	1039.81480	16.38266	412.37042	0.11455
25.81588	21.14334	13.86338	20.48287	69.33664	1039.80790	14.94212	367.13330	0.10198
25.81449	20.67000	13.84872	20.04705	69.08435	1039.79330	13.30592	311.10093	0.08642
26.11073	20.24566	13.84296	19.64895	68.77503	1039.72969	11.57111	254.46259	0.07068
26.73071	19.57787	13.81391	18.95932	68.49027	1039.72845	9.48903	184.14502	0.05115
28.42257	18.63131	13.77969	18.22576	68.06490	1039.80047	7.63720	115.51823	0.03209
29.31855	17.17124	13.73610	17.03905	67.61221	1039.78226	6.26963	68.71254	0.01909
26.37571	15.38611	13.66515	15.08524	66.72106	1039.89347	4.82146	32.22461	0.00895
26.29146	21.03353	15.74507	20.74793	61.68686	1039.53540	10.62881	219.37486	0.06094
25.82414	21.47645	15.78806	21.16407	61.83788	1039.49873	12.54927	285.78901	0.07939
25.68287	21.80957	15.80824	21.47687	61.93775	1039.49781	14.19275	338.79912	0.09411
25.75552	22.19518	15.81580	21.83652	62.08412	1039.52571	15.84202	392.39811	0.10900
25.92260	22.53380	15.82325	22.14556	62.14031	1039.58799	17.14376	433.30412	0.12036

Table 8: Calculations to determine the mass flow rate of air for the calibration of the hot wire anemometer.